Utrecht University
Faculty of Geosciences
Department of Earth Sciences

Master's Thesis in Earth Structure and Dynamics

Pore Scale Modelling of Gas Flow and Transport in Shale Rock Reservoirs

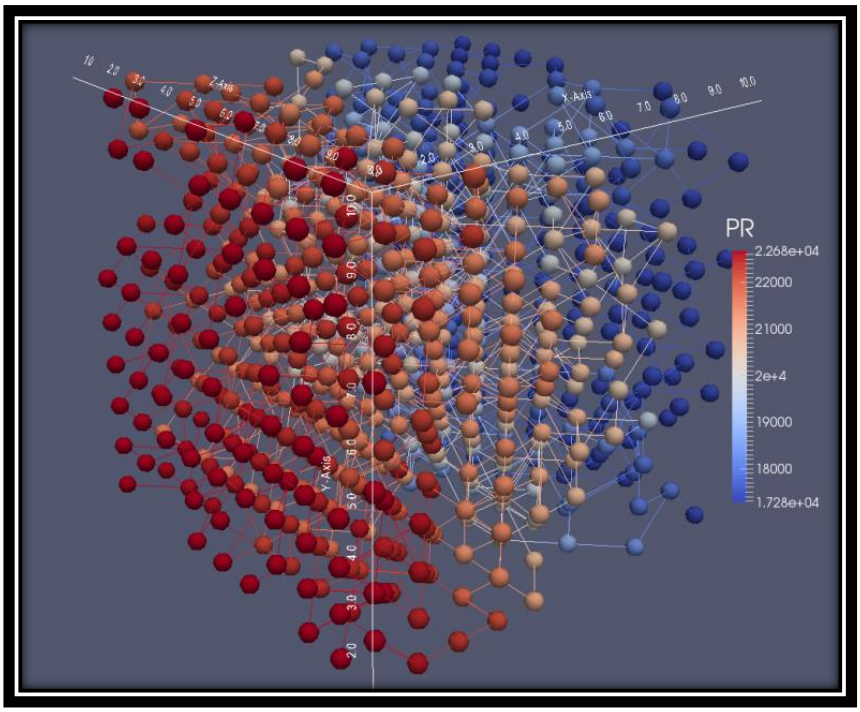

Author: **Vincent W.A. Vermaas**
Student number: **3345963**
Supervisor: **Dr. Amir Raoof**
Second Supervisor: **Prof. dr. Ruud Schotting**

Utrecht, October 2015

Abstract

Gas permeability of reservoir rock is of great interest in petroleum engineering, when considering the optimal extraction of shale gas. Gas shale contain a large fraction of nanopores that constitute gas stored mainly in the organic fraction by adsorption and in the pores of the rock matrix which lead to an apparent permeability that is dependent on pore pressure and pore structure. Shale gas flow is controlled by special flow mechanisms at different scales which make the prediction of shale gas transport more complex than conventional gas flow and transport. At the nano-scale pore, Darcy's law is not practicable anymore and gas flow may fall in flow regimes such as viscous flow, slip flow and Knudsen diffusion. The challenge is to understand and develop equations that describe the gas flow and transport in low permeability rock reservoirs (e.g. shales) and gain more understanding of the effect of declining field pressure and mean pore throat size distribution on the gas permeability using the pore network modelling. This thesis present a literature review and a newly developed pore network model called PoreFlow to simulate shale gas flow and transport at the pore scale. Gas flow and transport in a pore throat network and single pore throats at the nano-pore scale have been studied with emphasis on the K_{app}/K_d ratio of the shale gas matrix, thereby taking Knudsen diffusion and gas slippage into account.

This paper uses the analytical methods of Mehmani et al. (2013) and Javadpour (2009) and modifies the newly developed pore network model PoreFlow. The results indicate that apparent permeability is sensitive to reservoir gas pressure and pore throat sizes. For small pore throat sizes (i.e. <50 nm) and low pressures (i.e. <10 MPa), the K_{app}/K_d ratio is larger. The effect of the Knudsen diffusion and gas slippage on gas permeability is higher in smaller pore throat sizes (i.e. <20 nm) and at lower pressures (i.e. <20 MPa). Gas slippage has the primary effect at small pressures (p = 5 MPa - 10 MPa) and the highest contribution of the Knudsen diffusion effect is reached for pores in the range of 5 – 10 nm. In addition, the contribution of Knudsen diffusion is negligible for pores larger than 100 um which is the reason that, in conventional systems, Knudsen diffusion is not included in flow models. Moreover, gas permeability not only depends on the pressure gradient which drives the flow of gas but also depends on absolute pressure values in individual pores. Specifically, smaller pressures result in an increase in permeability. Furthermore, for complete validation of the PoreFlow model, measurements with similar pressures and pore throat diameters have been conducted and the model was found to match very well with the experimental data found in literature (i.e. Mehmani et al. 2013; Javadpour, 2009).

Pore Scale Modelling of Gas Flow and Transport in Shale Gas Reservoirs

Table of Contents

Section I: Introduction

1.1 Unconventional gas: An abundant natural gas resource

The growing maturity of shale gas plays led to a worldwide increased investment in unconventional gas exploration (i.e. shale gas). Unlike conventional gas, shale gas is trapped within the organic-rich shale source rock in interconnected pore space or adsorbed onto organic matter. It is extracted by fracturing the rock with a high pressure injection of a liquid to create cracks and ultimately release and extract the gas. Due to the many geological and economic factors, unconventional gas resources can be very complex and hard to extract. It requires a more advanced technological investment to extract the gas as opposed to conventional gas. One of the reasons is the low permeability of shales in the order of 10^{-22} m^2. This greatly inhibits the gas from migrating to more permeable rock. In conventional gas reservoirs, however, natural gas migrates from an organic-rich source formation into a permeable reservoir rock, where it is trapped by and overlying layer of low permeable rock. Commonly, the conventional gas is a lot easier to extract but harder to find, whereas unconventional gas is easier to find but a lot harder to extract. However, with recent technological improvements shale gas extraction is now economically viable and can be seen as a solution to the exceeding global energy demands. A mature understanding of shale properties is of great interest and necessity for acceptable production estimates.

A report of the U.S. EIA (2013) stated that 32% of the total estimated natural gas resources globally are in shale formations. Large-scale gas production is currently occurring highly in the USA and is expected to account for more than 50% of US's gas supply by 2020(Polczer, 2009). Giant shale gas recourses include the Barnett shale in Texas, USA, Marcellus Shale in the Appalachians, USA, Haynesville Shale in Louisiana, USA and Fayetteville shale, Arkansas, USA. Research on gas shale reservoirs in other countries than the US is available but rather incomplete.

1.2 Unconventional gas classification

Unconventional gas can be classified into three main types: (1) shale gas, (2) tight sands and (3) coal bed methane. The biggest difference between conventional and unconventional rock is permeability (**fig. 1**). Permeability is one of the most fundamental properties of any reservoir rock required for modelling hydrocarbon production [Sakhaee-Pour and Bryant, 2012]. Contrary to conventional reservoir rock, where permeability is only a function of topology and morphology of the pores, the permeability in shale depends also on pressure. Shales are fine grained, organic rich, sedimentary rock. It is composed mainly of clay-size mineral grains. Unlike conventional gas, shale formations act as both a source of gas and as its reservoir. It is easier to find but harder to produce. Gas is stored in shale in three forms; free gas in rock pores, free gas in local natural fractures, adsorbed gas onto organic matter and mineral surfaces. Tight sands are low permeable sandstones where the pore-throat sizes typically range from about 2 to 0.03 um in diameter [Nelson, 2009]. Coal bed methane refers to a form of natural gas that can be extracted from coal beds. Methane is adsorbed into the solid matrix of the coal. So, not only does the rock fabric controls the permeability (or transmissivity), but also the efficiency of gas flux through the microporous rock matrix.

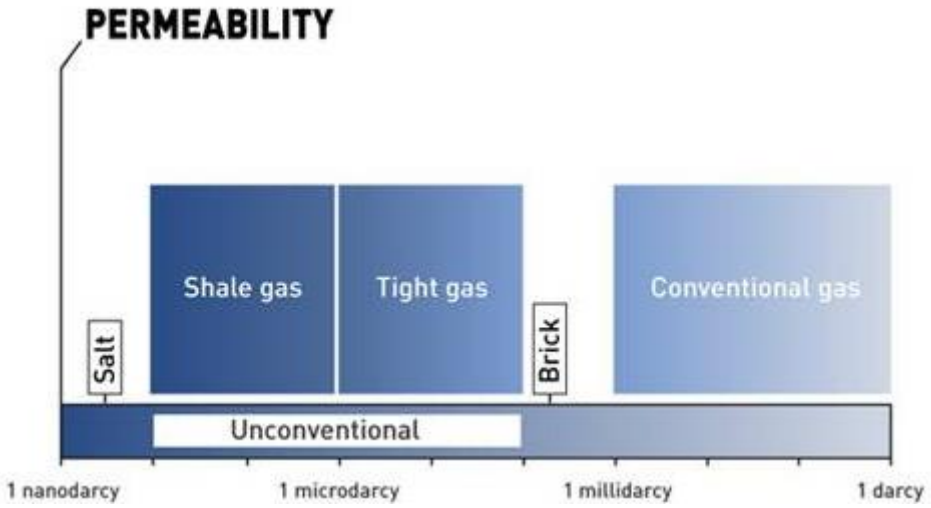

Figure 1: Permeability of shale gas vs. tight gas vs. conventional gas (source: www.total.com/en/energies-expertise/oil-gas/exploration-production/strategic-sectors/unconventional-gas)

1.3 Significance of Pore Network Modelling for shale gas research

Pore Network Modelling (PNM) is a field of study concerned with the analysis of the flow through porous media. It classifies the void space into pores and pore throats and investigates the interaction between the pores. The interaction take place through pore throats, which are often defined the narrowest region of the void space between to neighbouring pores. The pore size distribution and hydraulic conductance of the throats govern the overall flow properties of the PNM. This analysis is at pore-scale, which is smaller than the core-scale at which most lab measurements are reported in available research literature (**fig. 2**).

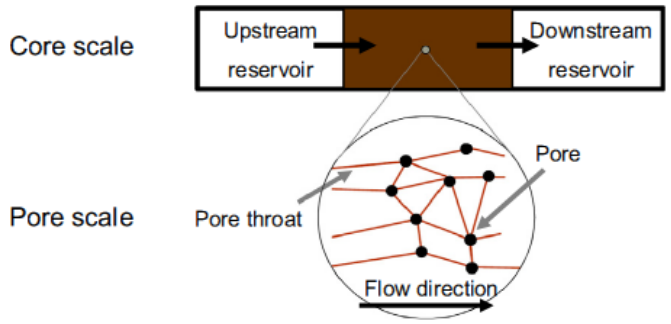

Figure 2: Schematic of the network modelling approach at pore-scale which is smaller than the core-scale (source: Sakhaee-Pour and Bryant, 2014)

Recently, there has been an explosion of interest in pore-scale modelling, with a variety of both petroleum and environmental applications. Pore-scale models are no longer limited to simple two-phase flow processes and the computation of relative permeability and can now be used as a platform to explore a huge range of phenomena [Blunt, 2001]. Also, it is now possible to represent the complex geometry of the pore space more adequately which leads towards truly predictive modelling which has proved elusive in the past.

Gas shale reservoirs are characterized to have very small pores with diameters in nanometre range that constitute gas stored in mainly in the organic fraction by adsorption and in the pores of the rock matrix [Bustin and Bustin, 2012; Wu, 2014]. As Shahimi and Tsotsis (2003) already pointed out, the significance of investigating the transport of fluids and gas inside nanoporous material is important to understand how a transport process takes place in their pore space so that their morphology can be optimized for such applications as separation and purification. Gas flow dynamics in general is an empirical science that relies heavily on experimentation and modelling to determine the effects of changes in parameters and thus understanding the flow mechanisms. Research institutes worldwide have addressed aspects of flow and transport of shale gas and outcome of experimental data is only increasing [e.g. Javadpour 2009; Freeman et al. 2011; Mehmani et al. 2013]. Transport and flow phenomena in porous media can be modelled according to simplified sets of equations which describe the complex properties of porous. However, different flow mechanisms at different scales make the prediction of shale gas transport more complicated and thus more challenging [Zhang et al. 2014]. The physics of gas flow in nanopores and shale rock permeability has not yet been fully understood because of the complexities involved in modelling flow through nanoscale throats. Knowing the flow behaviour in the nanoscale throats is of major importance for stimulation design, gas production optimization and calculations of the relative permeability of gas in shale gas systems [Wu 2014].

1.3.1 Challenges in pore scale modelling of shale gas

Shale gas flow is controlled by special flow mechanisms at different scales which make the prediction of shale gas transport more complex than conventional gas flow and transport. Gas transport in nanopores is a combination of several flow mechanisms including viscous flow, Knudsen diffusion and molecular diffusion [Civan, 2010; Javadpour, 2009; Jun et al. 2013]. In addition, these mechanisms depend on petrophysical properties such as pore size distribution, permeability, and pore connectivity. Classical simulation approaches based on Darcy's law may not be appropriate for simulating shale gas flow in shale [Ren et al., 2015; Zhang et al., 2014, Mehmani et al., 2013]. Inherent characteristics of gas shale such as widely dispersed organic matter and nano-scale pore system ensure that transport mechanisms not fully follow Darcy's law. Also, shale gas reservoirs contain a large fraction of nanopores, which lead to an apparent permeability that is dependent on pore pressure and pore structure [Guo et al., 2015]. For the porous systems with variable pore sizes, the apparent permeability is not only highly dependent on the fraction of nanopores but the pores' connectivity as well. Amann-Hildebrand et al. (2012) listed some key problems that is associated with the issue of why existing concepts and theories developed for conventional reservoirs cannot be readily transferred to unconventional reservoirs (i.e. shale rock, tight sands, CBM). (1) Low to extremely low permeabilities, (2) high capillary entry/displacement pressures, (3) Inadequacy of conventional multiphase-flow and relative permeability concepts, (4) Interference of gas sorption/desorption and solution/exsolution with transport processes, (5) Increasing importance of molecular diffusion relative to pressure-driven volume flow (Darcy flow). More information about the mechanisms and processes affecting transport and flow of shale gas can be found in Section II.

Another challenge is the computational power that is needed for simulation of gas flow in nano-pores. Fortunately, there has been an improved progress in the computational technology. Numerous of models have been developed over the years and with increasing computational power and computer storage capacity it is possible to model gas flow at micro- and nanoscale. However, when it comes to modelling, the complex flow geometries created by the massive hydraulic fracturing treatments required to make these wells commercially viable are very difficult to model and typically modelled incorrectly. Consequently, traditional production data analysis usually fails to render an accurate permeability for the reservoir [Freeman et al., 2011]

1.4 Research scope and Thesis overview

Various attempts have been made to model flow in shale gas systems. However, there is currently little understanding and general agreement regarding the impact of as Knudsen diffusion and gas slippage on flow behaviour in tight shale rock formations at the pore-scale.

The main research questions are;

- How will flow and transport at the nano-pore scale affect the large scale behaviour of shale gas
- Determine the apparent permeability of shale gas matrix and compare with Darcy permeability to analyse the effect of gas slippage and Knudsen diffusion in shale gas rock

The objective here is to simulate flow and transport of shale gas at the pore scale and capture the fundamental physics behind this process. The research question is how flow and transport at the pore scale affects the large scale behaviour of shale gas. Given the potential of pore network modelling I aim to model flow and transport of shale gas in low permeability rock using a new potential complex network modelling tool called PoreFlow. This study is conducted using capillary tubes at a nanoscale range, both single tube and network. After a comprehensive literature review and pore scale modelling I will compare my modelling results with results reported in scientific literatures. This proposed research will contribute to present day knowledge to enhance our understanding of shale gas simulations, in which gas flow in nanopores plays a critical role.

This work is organized as follows: In *Section II*, I present a literature review that summarize shale gas flow and transport mechanisms as well as the different approaches and models that is previously used by researchers to model pore network at micro- and nanoscale. *Section III* describes PoreFlow simulation parameters and PNM algorithm. In S*ection IV*, I present the results and will discuss those results with other available studies concerning shale gas flow and transport in rock.

Section II: Literature Review

2.1 Shale vs conventional rock

The main difference between shale and conventional rock is the large amount of nanopores that exist in shale rock and thus the permeability of the rock. Permeability gives an indication of the ability for both gas and/or liquid to pass through a rock sample. Intrinsic permeability depends only on the material structure of the rock. In shale formations, however, a function of pressure and temperature in addition to desorption must be used since the pore sizes within organic matter change as a result of Langmuir sorption that can be described as apparent permeability (Javadpour, 2007). Darcy's law cannot simply apply anymore at this very small pore-scale and terms like apparent permeability (Javadpour, 2007) is used to describe flow in shale systems. The challenge is to understand and develop equations that describe the gas flow and transport in lower permeability rock. Because of the very low permeability in shale (instead of the higher permeability in conventional rock) make this more of a challenge. Another important difference between shale and conventional samples is the pressure in the inlet and outlet. With shale you need to consider not only the pressure gradient (as it is in the case of conventional rock samples) but also the amount of pressure at the inlet.

Shale gas flow and transport mechanisms are the first and most important step for accurately simulating shale gas flow in shale. The flow ability of gas is affected by several inherent characteristics of gas shale, such as: gas composition, organic richness, geometry structure of the nanopores and, more fundamentally, the deviation of the gas flow from the description of continuum fluid mechanics [Zhang et al., 2014]. Unlike conventional gas reservoirs, gas flow in shale reservoirs is a complex and multiscale flow process which has special flow mechanisms. Shale gas reservoirs contain a large fraction of nano pores, which leads to an apparent permeability that is dependent on pore pressure, fluid type, and pore structure. In terms of fluid mechanics, the main differences between micropores (conventional reservoirs) and nanopores (unconventional reservoirs) can be broadly classified into two areas: non-continuum effects and dominant surface interactive forces. These two effects are negligible in cases of large pore sizes. Also, the effect of adsorbed gas is neglected in modelling flow through conventional rock. This because the occupied volume is negligible compared to the total void space in conventional rocks [Sakhaee-Pour and Bryant, 2012]. However, the adsorbed volume of gas is crucial in shale because the throats are often smaller than 10 nm and much of the void space is in the organic material, for which gas has a large affinity.

In section III, I will discuss these challenges and the methodology that will be followed to model gas flow and transport in shale gas. This section will discuss the mechanisms and processes that affect the transport and flow of shale gas in porous media using literature research. In addition, I will discuss the modelling approaches of shale gas and give a brief history of research that has contributed a better understanding in the dominant mechanisms that influences the flow and transport of shale gas.

2.2 Gas transport mechanisms in shale matrix

At equilibrium, gas molecules are distributed throughout strata. Gas molecules occupy pores as compressed gas, cover the surface of the kerogen materials as adsorbed gas and disperse in the kerogen materials as dissolved gas. When the equilibrium is being disturbed by drilling a well or inducing a fracture for instance, the gas molecules will start flowing toward the low pressure zone. Generally, gas flow happens first, followed by gas desorption and gas diffusion in kerogen (different from Knudsen diffusion). Overlaps for each of these processes are not uncommon [Javadpour et al. 2007].

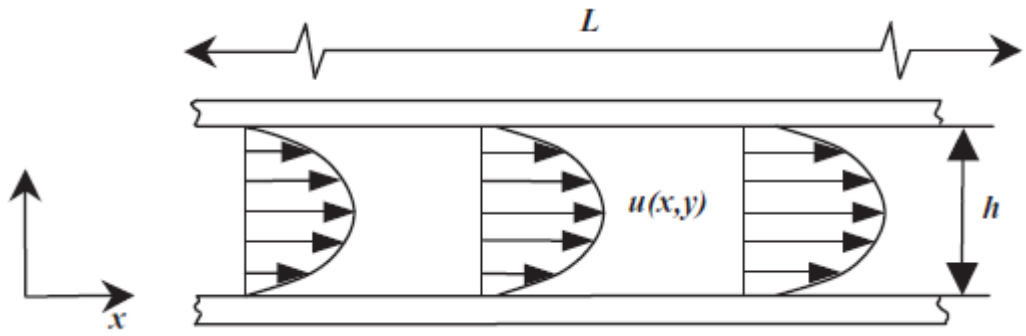

Figure 3: Geometry for pore throat analysis (adopted from Roy et al. 2003)

Under isothermal condition, output process of gas flow from low-permeability shale formations (e.g. shale reservoirs) can be described by a combination of mechanisms acting at different scales (Javadpour, 2009, Javadpour et al. 2007; Fathi et al. 2012; Freeman, 2010, Ozkan et al. 2010, Kuila et al. 2013). These are:

1. Desorption from kerogen and clay surfaces, and subsequent surface diffusion of the adsorbed gas molecules under a pressure gradient.
2. Knudsen diffusion and slip flow in micropores
3. Darcy flow in larger meso- and macropores

Most of the earlier studies employed kinetic theory based techniques to explain gas transport in nano-scales [Barisik and Beskok, 2014]. This was justified by matching the Knudsen and Mach numbers to maintain a so-called dynamic similarity between the low pressure and nano-scale gas flows. Unfortunately, this approach neglects the nano-confinement effects, which become increasingly important with the reduced length scales [Barisik and Beskok, 2014]. Flow of gases in tubes (including capillaries) is described by Hagen-Poiseuille equations with no-slip boundary conditions. The no-slip boundary condition indicates viscous bonding of fluids to the wall and is modelled by assuming the particle velocity to be zero at the wall of the pore. The interaction between gas and wall molecules determines flow physics in the near wall and bulk flow region [Barisk and Baskok, 2014]. Viscous flow and Knudsen diffusion refer to an individual gas species and occur when gas moves in a porous medium (**fig. 3 and 4**). Molecular diffusion refers to the relative motion of different gas species and only occurs in multicomponent gas transport in porous media [Jun et al. 2013].

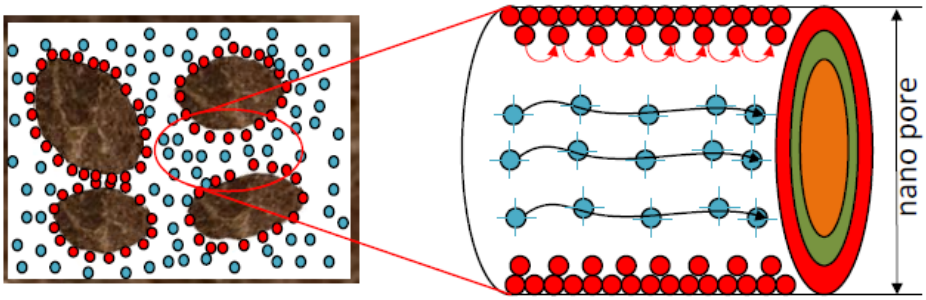

Figure 4: Gas flow mechanisms in nanopores showing the movement of a single component gas through a porous medium. Red represents Knudsen diffusion and blue represents viscous flow [source: Guo et al. 2013].

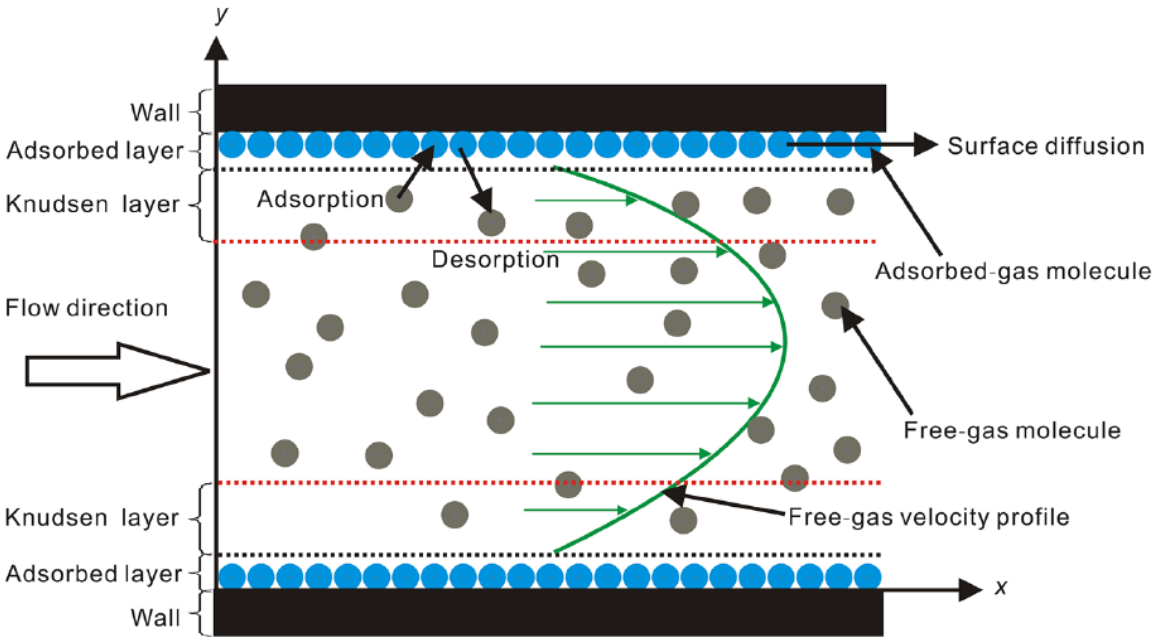

Figure 5: Schematic of shale gas flow in a kerogen pore [source: Ren et al. 2015]

Viscous flow (or Darcy flow) occur when the gas mean fee path is smaller than the pore throat diameter at which then the motion of gas molecules is determined by their collision with each other. Viscous flow is the primary driver of gas flow and can be modelled using the Darcy's law Very small gradients in pressure will cause net flux exceeding the flux generated by steep concentration gradients [Freeman et al., 2011; Thorstenson and Pollock 1989].

2.2.1 Diffusion

Gas diffusion, however, is an important mechanism in low permeability gas reservoirs and is typically modelled by Fick's law, which relates concentration gradient to flux. The lower the permeability, the stronger the diffusion influence [Wei et al. 2013; Ayala et al. 2007]. Knudsen diffusion attempts to describe a physical process of the motion of gas particles inside a porous solid [Fiedler et al. 2011]. With smaller pores and pore throats means, diffusion begins to play as a more dominant transport mechanism.

Besides Knudsen diffusion there is also surface and liquid diffusion. Surface diffusion occurs where molecules are adsorbed to the surface of the porous medium and move along the surface. Shale is known to contain a quantity of adsorbed gas on its kerogen and clay surfaces, so adsorption is certainly an important contributor to total gas storage and it may also be an important transport mechanism (Akkutlu and Fathi, 2012; Freeman et al., 2011). Liquid diffusion is the transport of (dissolved gas) molecules through a liquid phase with concentration gradient as the driving force. It is known that both tight gas and shale gas reservoirs contain water, but the water is typically found at saturations below the irreducible saturation. A liquid hydrocarbon phase may be present in tight gas or shale gas reservoirs, which may be due to the thermodynamic equilibrium or capillary condensation (Hassan and Way, 1996). This research neglect surface and liquid diffusion and focus mainly on Knudsen diffusion as a major contributor to gas flow in shale rock. Whether the flow is dominated by viscous flow or Knudsen diffusion depends on the relationship between the mean free path of gas and the pore size of the porous media. Several studies already showed the Knudsen diffusion as the dominant mechanism in shale gas [Javadpour, 2009; Sakhaee-Pour and Bryant, 2012 etc.]. This because the pore diameter reaches the same order as the gas molecular mean free path at which collision between molecules and the pore walls become more important than by viscous flow [Jun et al.]. The collision between gas molecules and the wall becomes the dominant effect [Javadpour, 2009; Guo et al., 2015].

2.3 Gas flow regimes

Description of various gaseous flow regimes through tight porous media has drawn considerable attention since Darcy´s law cannot realistically describe the variety of the relevant flow regimes [Civan 2010; Javadpour et al. 2007; Javadpour 2009; Mehmani et al. 2013]. Non-equilibrium gas flows are classified by the Knudsen number (eq. 2), which is a non-dimensional parameter indicating the rarefaction of the flow of which the ratio is the gas mean free path to the characteristic microfluidic length scale [Barisk and Beskok, 2014].

$$Kn = \sqrt{\frac{\pi y}{2}\frac{M}{Re}} \qquad \text{Eq.2}$$

Where *M* is the Mach number and *Re* is the Reynolds number and *y* is the specific heat ratio. Fluid flow behaves differently at various Knudsen numbers. Based on the value of Knudsen number, gas transport in porous media can be divided into four flow regimes (Figure 1)

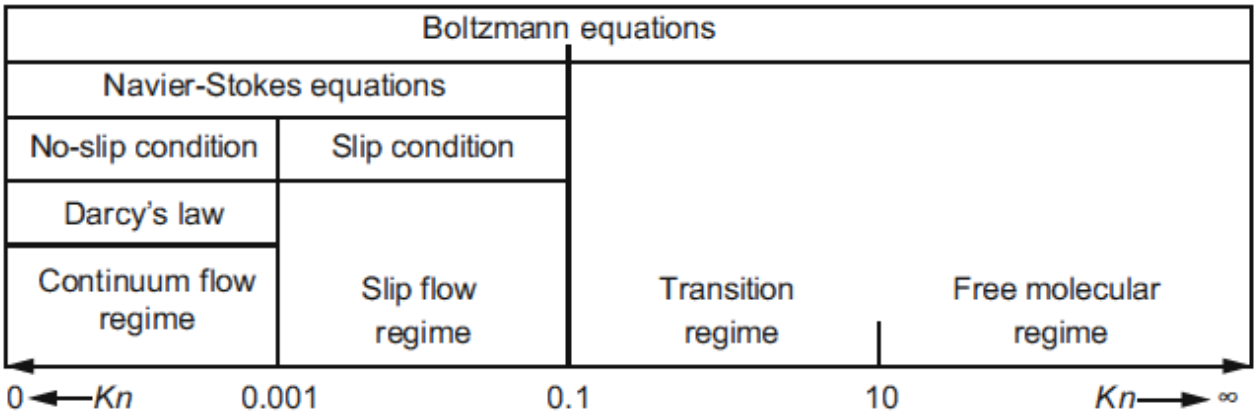

Figure 6: Classification of the gas flow regimes and governing equations based on the Knudsen number [source: Jun et al. 2013].

Figure 6 shows that, depending on the Knudsen number, gas transport is considered in the continuum (Kn < 0.01), slip (0.01 < Kn < 0.1), transition (0.1 < Kn < 10) and free-molecular (Kn > 10) flow regimes. The Knudsen number is almost in the range of 0.001 and 10 within all the pressure from 0.1 to 10 MPa when the pore diameter is less than 1 µm, so the main gas transport regime of shale nanopores is the slip flow regime and the transition regime (**fig. 7**). Therefore, both the viscous flow and Knudsen diffusion have a great impact on the gas transport in nanopores and, again, the Darcy equation cannon be simply used to describe gas transport in nanopores. Important to note is that the Knudsen diffusion is the dominant mechanisms in transition and free molecular flow regime, whereas viscous flow is the dominant mechanism in continuum and slip flow regime. Knudsen diffusion and viscous flow can be ignored in continuum and free molecular flow regime and is therefore not considered.

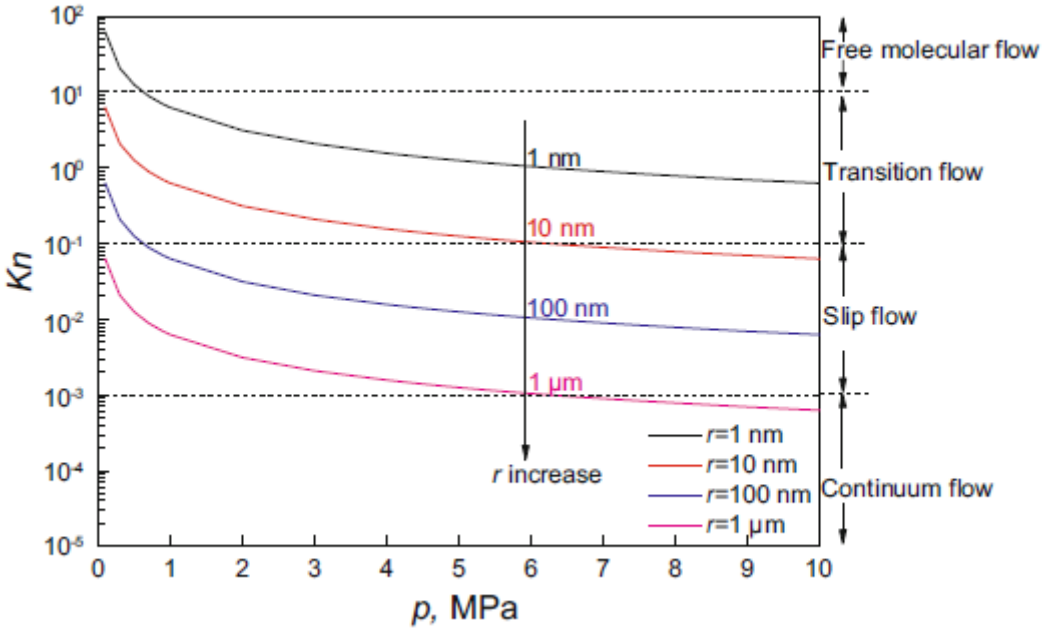

Figure 7: The Knudsen number and gas flow regime at different pressures and pore diameters (source: Jun et al. 2013).

2.2.1 Continuum flow vs slip flow

Zhang et al. (2014) showed that the slip effect significantly increases the flow rate in the tube. In addition, the velocity profile of the tube show changes from the parabolic to a flat shape for the total slip boundary (**fig 8**). This indicates that the flow mechanism no longer follows Poiseuille's law and classical flow theory cannot be used to calculate the flow velocity profile and permeability.

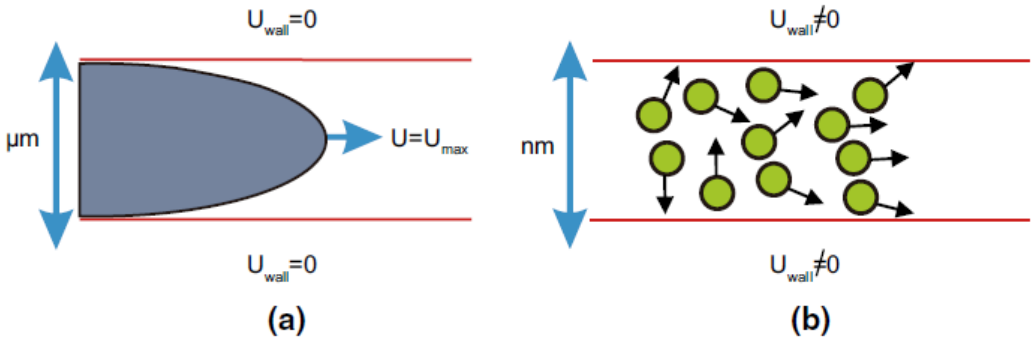

Figure 8: Velocity profile for (a) continuum flow, (b) slip flow (source: Zhang et al. 2015)

In terms of velocity equations, there are two different boundary conditions; Continuum flow and slip flow (Zhang et al., 2014 and Javadpour, 2009]. The classical continuum model assumptions where momentum transfer by means of bulk phase viscosity, fluid velocity matches solid velocity at walls cannot always provide accurate results. For continuum flow, mass flux depends on the proportional constant K, so-called absolute permeability (in mD) of the rock (eq. 3 and 4):

Mass flux caused by pressure difference; $$J_{a\_no\_slip} = -\frac{\rho_{avg} r^2}{8\mu} \times \frac{\nabla p}{L}$$ Eq. 3

With absolute permeability; $$K_{no\_slip} = \frac{r^2}{8}$$ Eq. 4

Where r is the radius of the pore in m, μ is the viscosity in Pa/s, ∇p is the pressure gradient, L is the pore length in m and ρ_{avg} is the average density in kg/m^3. In the slip flow regime, gas slippage occurs where the mean free path of the gas molecules is in the order of the characteristic pore size of a porous medium. This phenomenon leads to Klinkenberg's effect where the measured permeability of a gas (apparent permeability) is higher than that of the liquid (intrinsic permeability) [Chen et al. 2015; Fathi et al. 2012; Klinkenberg 1941].

Klinkenberg (1941) demonstrated that, under steady state and laminar flow condition, the permeability of rock formations that contain gas is a linear function of pressure. Klinkenberg defined the interaction by a very small layer known as the Knudsen layer which is thinner than the molecular mean free path where only molecule to wall collisions occurs rather than molecule to molecule collisions of which the last one can be ignored. Using the Klinkenberg's approach, the slippage velocity captures this molecule to wall collisions contribution and when the velocity is zero, a Hagen-Poiseuille type of velocity profile is acquired. Note that the approach is acceptable for Knudsen numbers 0.01 – 0.1. Klinkenberg ignores the transition flow regime since molecule to wall collisions and collisions among the molecules itself play a significate role.

So, for slip flow in nano-scale pores, the ratio of molecule to wall collusions to molecule to molecule collisions increases with an increasing Kn. The pore wall is no longer zero so the mass flux can be described as shown in equation 5 and 6. However, in the slip flow regime, the molecule to molecule interaction is still dominant.

$$J_{a\_slip} = -F \times \frac{\rho_{avg} r^2}{8\mu} \times \frac{\nabla p}{L} \quad \text{Eq. 5}$$

With $$F = 1 + \sqrt{\frac{8\pi RT}{M}} \times \frac{\mu}{p_{avg} r} \times \left(\frac{2}{\alpha} - 1\right) \quad \text{and} \quad K_{slip} = F \times \frac{r^2}{8} \quad \text{Eq. 6}$$

Where *F* is a theoretical dimensionless coefficient, *R* is the gas constant in J/mol/K, *T* is the temperature in K, *M* is the molar mass in kg/kmol, ρ_{avg} is the average pressure in Pa, r is the pore radius in m, *L* = pore length in m and α = the tangential momentum accommodation coefficient.

2.2.2 Transition vs Free molecular flow regime

The physics of the transition flow regime is complicated and most models are used to predict the computational results of the Monte Carlo simulations [Karniadakis et al. 2005]. It implements different shear stress laws in the Navier Stokes equations and Klinkenberg correction cannot be employed for higher Kn flow regimes [Sakhaee-Pour and Bryant, 2012]. Free molecular regime is relevant for gas-phase transport at ambient conditions. The mass-flow rate of the free molecular regime was modelled by Knudsen (1909);

$$J_{Kn} = -D_{Kn} \nabla n_i \quad \text{Eq. 7}$$

Unlike ordinary diffusion, only one component is considered to predict the flow rate in this mechanism which requires Knudsen diffusivity.

2.4 Pore size distribution and pressure differences on gas flow regimes

If the pore-with is large relative to the mean free path of the gas molecules (at high pore pressures and large pore radii), there are two major types of mass transport mechanisms. Total pore pressure gradient exists and mass transport may take place as a result of Poiseuille flow. If a partial pressure gradient exists, mass transport may take place as a result of molecule-to-molecule collision (i.e. molecular diffusion). Molecular diffusion is not applicable for single-phase gas flow as the partial pressure will always be equal to one. If the pore-width is small relative to the mean free path, mass transport occurs as a result of molecule-to-wall collision in the presence of either a total pressure or a partial pressure gradient (Knudsen diffusion or molecular flow) [Kuila et al. 2013]. Furthermore, the nature of gas flow changes when the average pressure inside the capillary is reduced. Also, smaller capillaries results in much higher fluid flow velocities than predicted by the Klinkenberg slippage theory. This raises concerns in regards to the nature of dominant mechanisms. Fathi et al. (2012) show that in the case of capillaries under 50 nm one needs to be more careful because the variations in average velocity are higher than what analytical methods and Klinkenberg's slip theory predicts. Also, a portion of the gas remains adsorbed in shale. The amount depends on the prevailing pressure

and adsorbent (e.g. kerogen in shale) conditions [Civan et al. 2011]. This can be estimated by means of the Langmuir isotherm;

$$q_a = \frac{q_L p}{p_L + p} \qquad \text{Eq. 8}$$

Where *q* is the flow rate, *p* is the pressure in Pa and *L* is the pore length in m.

2.5 Modelling approaches of shale gas flow and transport

A network model should aim at a good representation of pore and throat interconnectivity in a porous medium. While pores and throats can be described via simple geometrical shapes, the models should retain a subset of the realistic (microscale) properties e.g. pore/throat sizes and coordination number distribution. The first use of a network of pores to represent multiphase flow in porous media was by Fatt (1956b), where he introduced the notion of interconnectivity. Since then, researchers have attempted to derive an equation to characterize the law of gas flow and to simplify simulation work. In the 1980's, percolation theory was used to describe multiphase flow. In the 1990's, interest in pore-scale modelling had decreased due to the fact that something more than percolation-type models and simple pore-space geometry was needed to develop models to explain the whole range of flow and transport phenomena in porous media. Fortunately, in the 2000's, there was an increased interest and development in models. Table 1 shows a brief history of gas-flow models throughout time. Reviews on network flow models can be found [Blunt, 2001 and Joekar-Niasar and Hassanizadeh, 2012].

Table 1: History of gas-flow models in porous media and shale systems (from Naraghi and Javadpour, 2015)

Author	Methods
Klinkenberg (1941)	Empirical slip flow
Brown et al. (1946)	Theoretical slip flow
Javadpour (2009)	Maxwell slip flow, Knudsen diffusion, single straight nanotube
Civan (2010)	Simplified 2nd order slip model, several empirical parameters
Darabi et al. (2012)	Maxwell slip flow, Knudsen diffusion, surface roughness, average pore size
Akkutlu and Fathi (2012)	Circular pores in organic matter and slit-shape pores in inorganic matter
Mehmani et al. (2013)	Network model of straight nanotubes with Maxwell slip and Knudsen diffusion
Rezaveisi et al. (2014)	Maxwell slip and Knudsen diffusion for multicomponent chromatographic separation
Singh et al. (2014)	Non-empirical model, circular and slit-shape pores in organic matter
Naraghi and Javadpour (2015)	Maxwell slip flow, Knudsen diffusion, surface roughness, PSD in organic and inorganic, TOC, sorption

Different modelling approaches have been adopted to simulate gas flow characteristics in nanotubes. Beskok and Karniadakis (1999), for instance, developed a unified Hagen-Poiseuille type equation covering the fundamental flow regimes in tight porous media including continuum fluid flow, slip flow, transition flow and free molecular flow conditions, while Klinkenberg (1941) introduced the Klinkenberg coefficient to consider the slip effect that was observed and Javadpour et al. (2007) proposed the concept of apparent permeability where Florence et al. (2007) made an attempt at utilizing the Hagen-Poiseuille type equations to derive a general expression for the apparent gas permeability of tight porous media.

2.5.1 Molecular dynamics

Several transport models have been developed to quantify gas transport in tight porous media with nanometre-size pores [Jun et al. 2013, Beskok and Karniadakis, 1999; Civan, 2010; Civan et al. 2011; Ho and Webb, 2006, Javadpour, 2009). A simple approach is to imagine diffusion in a single, typical pore, and to compute diffusion coefficients using molecular dynamics (MD). Many research used this as the basic approach [Cai et al. 2008; Liu et al. 2012]. The MD method is a useful tool and is able to give details on the gas flow , such as the velocity profile in the nanopores. Pressure-driven gas flows can be simulated by forming a density gradient along the stream wise direction. However, this requires modelling of long nano-channels with inlet and outlet reservoirs at different gas densities and pressures [Barisik and Beskok, 2014]. Such approach is not feasible using MD. A more realistic approach is using a pore network model (PNM) [Cai et al. 2008]. In general, the MD/PNM approach with pore size distribution, is a suitable method when it comes to predicting diffusion in real nanoporous carbons, although it does not completely grasp the actual structure of the carbon found in nature. Although MD is theoretically suitable for simulating interaction in small-scale pores, it is not practical for simulating the nanoscale pore networks of shale because of the very high computational cost. Most MD calculations are limited to 10^{-15} s' time step, and results are limited to a very short time scale of ns. [Zhang et al. 2014]. High computing power and storage capacity of computers necessary

2.5.2 Lattice Boltzmann method vs Pore Network Modelling (PNM)

The two best known methods for pore scale modelling in porous medium are pore network models (PNM) [Fatt, 1956b] and Lattice-Boltzmann method [Sukop and Thorne, 2006]. The most popular approach for computing single and multiphase flow directly on pore-space images is the Lattice-Boltzmann method. This is a particle based technique that simulates the motion and collision of particles on a grid; the averaged behaviour can be shown to approximate the governing Navier-Stokes equation. This method is relatively easy to code and is ideally suited for parallel computing platforms [Blunt et al. 2013]. It shows to be a powerful tool to study flow and transport processes at the pore scale. However, Lattice-Boltzmann models developed for rarefied gas flows have difficulty in capturing the nonlinear relationship between shear stress and strain rate within the Knudsen layer [Zhang et al. 2006]. Also, Lattice-Boltzmann models are expensive in terms of both computational storage and run-time requirements [Raoof, 2011] and little work has been done to use Lattice-Boltzmann modelling on real porous media.

Another well-known method is pore network modelling pioneered by Fatt (1956b), who exploited the analogy between flow in porous media and a random resistor network [Fatt, 1956b]. Here, fluid flow and solute transport processes are simulated directly at the microscopic scale without assuming a priori the traditional macroscopic equations (e.g. Darcy's law). Simplified geometries and pore distribution are chosen to describe the topology of the porous structure [Laudone et al. 2008]. Further advances in network modelling only occur recently over the past two decades when computer processing power became more available. Since then the models have grown hugely in sophistication and now can accommodate many complicated flow mechanisms as well as a variety of different physical processes. It is now also possible to simulate gas flow by making adaptations in available models. A variation of gas flow models can be found in **Table 1**. Compared to other pore scale modelling methods, including Lattice-Boltzmann, pore network models are computationally effective [Raoof, 2011]. In addition, recent advances in PNM have allowed to model a degree of irregularity in channel cross-sectional shape that was not available in earlier models. Another important aspect is that pore network models are capable of capturing important statistical characteristics of porous media such as pore size distributions, together with coordination number distributions and topological parameters such as Euler number [Raoof, 2011]. Raoof (2011) used such a complex pore network model to simulate flow and transport in porous media.

2.5.3 Dusty gas model (DGM)

Mason and Malinauskas (1983) proposed a theoretical explanation for empirical observations that adopts a linear combination of gas-transport mechanisms to predict the overall flow rate. Simply said, this model describes the action of the porous material as that of a number of large particles having zero velocity in all directions at all times, dispersed throughout the proposed gas mixture. However, it avoids any assumption about the exact internal structure of the porous material [Webb and Pruess, 2003; Freeman et al. 2011]. The slip flow regime can also be simulated using the dusty gas model. This model adopts a linear combination of gas-transport mechanisms to predict the overall flow rate.

2.6 SEM imaging of internal structure of gas shales

One inherent characteristic of shale gas is its nano-scale pores. Several studies have investigated and tried to visualize the internal structure of gas shales at nanometre scale. The most widely applied method is scanning electron microscopy (SEM) [e.g. Dewer et al. 2012; Chen et al. 2013.; Blunt et al. 2013] that routinely produces images down to resolutions of nanometre sizes and capture 2D information. This is sufficient to image the pore spaces in even low permeability sandstones and carbonates and can also study the nm-scale pores in unconventional shale gas and shale oil reserves. The only problem is that the images are two-dimensional and hence the three-dimensional connectivity of the pore space is unknown [Blunt et al. 2013]. A more recent technology called FIB/SEM (focussed ion beams) acquires very high resolution three-dimensional images of very small rock samples (typically a few micrometres across). The ion beam makes very fine slices through the sample, enabling sequential SEM images to be obtained. The method is destructive but reveals unrivalled detail of small pore spaces [Blunt et al. 2013].

However, only a few studies have focused on the quantification of the geometrical information of individual pores in kerogen [Chen et al. 2013]. FIB-SEM is often used to obtain a 3D internal structure of kerogen in shales. The Barnett shale shows for example by using FIB/SEM micro Darcy values for local pore clusters. Kerogen particles display sizes higher than 0.5 micrometre are more commonly connected than smaller sized particles that are more likely to be isolated [Peng et al. 2014]. Loucks et al. (2012) and Curtis et al. (2011) mention that recent high resolution imaging studies using SEM have shown that matrix pores in shale consist of interparticle, intraparticle and organic matter intraparticle pores with sizes from the order of micrometre (interparticle pores) down to the range of 3 – 100 nm for intraparticle pores.

Section III: Pore Network modelling

Many published studies for fluid flow in nanopores are under extreme simple conditions where nanopores are mostly straight channels or nanotubes. Now it is in general agreement that very small pores (nanopores) exist in shale. At the nanopore scale, Darcy's law is not practicable anymore and Knudsen diffusion model is generally used. Similar previous studies concerning gas flow in nano pores have thus far focused on flow in a single channel (Javadpour, 2009; Freeman et al. 2011), a simple 2D network of channels (Sakhaee-Pour and Bryant, 2012), a combination of pores with nanometre and micrometre sizes with different flow physics mechanisms on both scales (Mehmani et al. 2013) or gas flow through nano-membranes (Guo et al. 2015). The challenge is to understand and develop governing equations to describe gas flow in these small pores. Javadpour (2009) present new formulations for gas flow that include some complexities that were ignored in developing the Darcy equations. Rather than using empirical correction factors in the Darcy equation, Javadpour (2009) suggest a rigorous theoretical approach to describe gas flow in nanopores of mudrocks and finally come up with a final formulation that is compatible with the Darcy equation for ease of adoption in commercial reservoir simulators. Mehmani et al. (2013) established a multi-scale pore-network with a constant coordination number of 4 by extracting pore-network from a dense random pack of spheres by Delaunay tessellation method, and the results show that gas flow in shale matrix is mainly determined by nano-pore fraction.

This research more or less follows the methodology of Mehmani et al. (2013) using equations and data provided by Javadpour (2009), Mehmani et al. (2013) and Sakhaee-Pour and Bryant (2012). The pore size distribution and hydraulic conductance of the throats govern the overall flow properties of pore network modelling. In this section, I start with a brief description of the simulation tool PoreFlow followed by an explanation of the modifications that were used in the model for simulating gas flow and transport. Then, results from the model will be presented and discussed.

3.1 Pore-network modelling using Poreflow

In this study, a complex pore-network modelling tool called PoreFlow is used that represent porous media and to perform flow and solute transport simulations in such a network (Raoof et al. 2013). A list of all the computational features of PoreFlow can be found in Raoof et al. (2013). The PoreFlow modelling method uses a Multi-Directional Pore-Network (MDPN) and is based on a regular cubic lattice network, which has two elements; pore bodies located at the regular lattice points and pore throats connecting the pore bodies, both with finite volumes (**fig 9**).

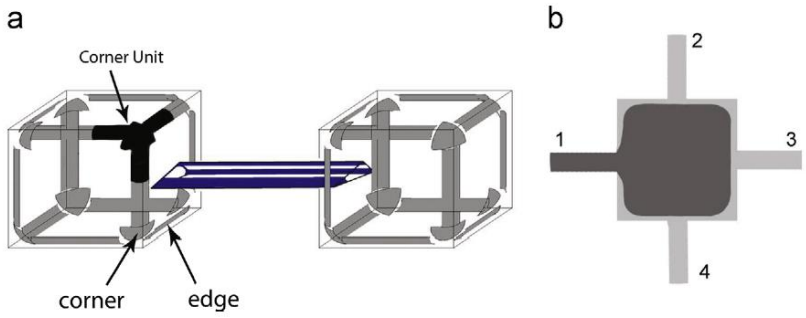

Figure 9: Example of (a) a two drained pore-bodies connected to each other and (b) a pore body which is invaded by the nonwetting phase (dark grey) through one of its throats and, as a result, reduces connectivity of the neighbouring saturated pore throats [Source Raoof et al. 2013].

For incompressible, steady-state flow, the sum of discharges into and out of a pore body, or a pore-body corner unit in the case of a drained pore body, must be zero. The continuity equation for the pore bodies can therefore be written as;

$$\sum_{n=1}^{N_{edge}^{CU,i}} q_{i,n} + \sum_{j=1}^{z_i} q_{ij,tot} = 0; \quad j = 1,2,\dots,z_i \tag{1}$$

Where $q_{i,n}$is the volumetric flow rate through pore throat *i*, $q_{ij,tot}$ is the total volumetric flow rate through pore throat *ij*, z_i is the coordination number of pore *i* and $N_{edge}^{CU,i}$ shows the number of edges through which corner unit I, within a drained pore body, is connected to other corner units, n, within the same pore body.

The pore space is represented by the pore bodies and pore throats utilizing a MDPN generator where pore throats can be oriented in 13 different directions, allowing a maximum coordination number of 26 that is possible in a regular lattice in 3D space with user-defined directional connectivities for anisotropic pore networks. Together with geometrical distributions of pore sizes it allows to mimic the microstructure of real porous media. To get a desired coordination number distribution, an elimination procedure is used to rule out some of the connections. The elimination number procedure is such that a pre-specified mean coordination number can be obtained. It involve that a bond had two possible states (i.e. open and blocked) assuming that each bond's state is random and independent of its neighbours. After a set of 13 threshold numbers (pi, i=1, 2, 3, …13) is determined, a random elimination number is generated with uniform distribution for each and every possible bond. If this elimination number is greater than the threshold number of the corresponding direction, the bond's state is assigned to blocked or vice versa. The larger the threshold number, the more chance for an open (connecting) bond in direction number i.

A network can be generated with a pre-specified mean coordination number by choosing a common threshold number for all directions. When threshold numbers are chosen to be different, different directions can be created which can result in anisotropic lattices. A given pore with coordination numbers of zero losses all its connection during the eliminations process and will be eliminated from the network structure. Pore bodies with coordination number of one could be eliminated when dead end pores are not considered except if they are located at the inlet or outlet boundaries. As fluid can only flow through open bonds, below the (critical) pc value the lattice will have zero conductivity. While above the pc value, the conductivity will increase as pi increases. Hence, there is a strong

relation between connectivity of the elements (i.e. microscopic properties) and the physical properties of the entire system (i.e. macroscopic properties) [Raoof, 2011]. Another approach to generate pore structures is to construct regular-pattern network. Regular-pattern networks are constructed by eliminating all the connections along some specific directions. A network can be equivalent to the bundle-of-tubes model, or the network is a commonly used regular structure network with connections only in principal directions, or networks with connections in diagonal directions, in 2D and 3D domains [Raoof, 2011; Raoof et al. 2013]

3.2 Network Flow Model (Methodology)

To simulate drainage process, the non-wetting phase (in this case gas flow) is considered to enter the network through an external reservoir which is connected to the inlet side of the network. The displaced phase escapes through the outlet face on the opposite side (**fig. 10**).

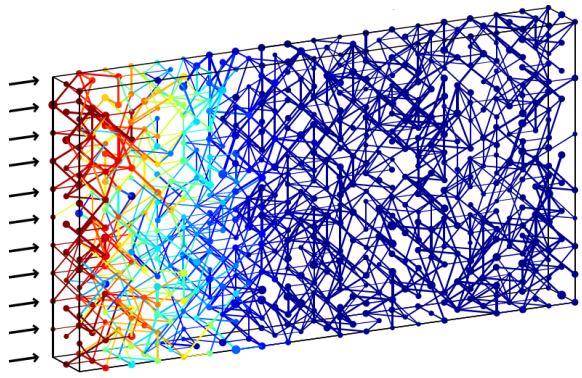

Figure 10: Example of a schematic of a pore network domain (source: Raoof et al. 2013).

Here it is assumed that the progress of the displacement is controlled by capillary forces. At every stage of the process, non-wetting phase invades all accessible pore bodies and throats with the lowest entry capillary pressure. The invading gas enters and fills an available pore throat only when the injection pressure is equal to or larger than the entry capillary pressure of the pore. Also, the basic assumption of modelling single-phase flow in a network of pores and throats is that the resistance to flow in the pores can be neglected as the diameters of the pores are greater than those of the throats [Mehmani et al. 2013]. If a channel is completely filled with a single fluid, the flow rate along the channel from pore I to pore j is given by the following formula;

$$q_{ij} = g_{ij}(p_i - p_j) \tag{2}$$

Where g_{ij} is the throat hydraulic conductivity, p_i is the pressure in pore I in Pa and p_j is the pressure in pore j in Pa. In this study, the recently existing pore network modelling tool PoreFlow is being used for shale gas modelling. So, in steady-state modelling, mass balance is enforced at each pore. Enforcing mass balance at each pore, together with the set pressures at inlet and outlet boundaries and no-flow at all the others, results in a system of linear equations on pore pressures. Important to note is that fracture pores in shale will not be modelled, but multiscale network modelling can be modified to include (nano to macro)fractures as well in future research .

3.2.1 Diffusive-advective gas flow in a tube

One of the intriguing problems in the field of gas-producing strata is the higher than expected gas production from reservoirs. To address this problem, apparent permeability and Darcy permeability is divided; $\frac{k_{app}}{k_D}$ (3)

A pressure dependent permeability function is then formulated (eq. 4), which is referred as the apparent permeability where Knudsen diffusion and slip flow is assumed to be the main contributors to the overall flow in porous media. Gas flow due to Knudsen Diffusion in a nanopore [Javadpour, 2009];

$$J_D = \frac{MD_K}{10^3 RT}\nabla p, \qquad with\ D_K = \frac{2r}{3}\left(\frac{8RT}{\pi M}\right)^{0.5} \tag{4}$$

Where M is molar mass, D_K is the Knudsen diffusion constant, R is the gas constant and T is absolute temperature in Kelvin. Gas flow due to pressure forces in a nanopore can be derived from Hagen-Poiseuille's equation as follows [Javadpour, 2009];

$$J_a = \frac{r^2}{8\mu}\frac{\rho_{avg}}{L}\Delta p \tag{5}$$

Where J_a is the mass flux for an ideal gas in laminar flow in a circular tube with negligible length of entrance effect, μ is flow velocity and ρ_{avg} is in kg/m3. Brown et al. (1946) introduced a theoretical dimensionless coefficient F to correct for slip velocity in tubes as follows;

$$F = 1 + \left(10^3 \times \frac{8\pi RT}{M}\right)^{0.5}\left(\frac{\mu}{p_{avg} r_{ij}}\right)\left(\frac{2}{\alpha} - 1\right) \tag{6}$$

At the second equation; α is the tangential momentum accommodation coefficient (varies from 0 to 1 depending on wall-surface smoothness, gas type, temperature and pressure), which is the portion of gas molecules reflected diffusely from tube wall relative to specular reflection [Maxwell, 1995] and ρ_{avg}= average pressure in the system.

$$\alpha = 1 - \log(1 + K_n^{0.7}), \qquad \text{with } K_n = \frac{labda}{r_{avg}}\ \text{(Knudsen number)} \tag{7)(8}$$

The overall mass flux equation for gas flow in a cylindrical tube is governed by a combination of Knudsen diffusion (Roy et al. 2003) and gas flow due to pressure forces (Javadpour, 2009; Brown et al. 1946; Bird et al. 2007; Mehmani et al. 2013; Shabro et al. 2009). Also, for slip flow in nano-scale pores, pore wall are no longer zero so the mass flux can be described as follows [Mehmani et al. 2013]:

$$J_{ij} = -\left[\frac{2r_{ij}M}{3\times 10^3 RT}\left(\frac{10^3 RT}{\pi M}\right)^{0.5} + \frac{Fr_{ij}^2\rho_{avg}}{8\mu}\right]\left(\frac{p_i - p_j}{L}\right) \tag{9}$$

Here, J_{ij} = mass flux, r_{ij} = the nanotube radius at inlet *i* and outlet *j* respectively, R = gas constant (8,314), T = temperature, M = gas molar mass, ρ_{avg} = gas average density ($\frac{p_i + p_j}{2}$), μ = gas viscosity at atmospheric pressure, p_i and $p_j$are pressures at the inlet and outlet of the nanotube, L = length of the nanotube. The first term in the bracket represents diffusive flow and the second term in the

bracket represents no-slip/slip gas flow due to pressure forces [Javadpour, 2009]. Finally, reference Darcy permeability K_D is computed using the no-slip Hagen-Poiseuille equation for volumetric flux through every throat [Mehmani et al., 2013];

$$k_D = \frac{\pi r_{ij}^4}{8\mu} \frac{(p_i - p_j)}{L} \tag{12}$$

The reference value serves to show the deviation of apparent permeability from the value one would compute if linear dependence of flux and pressure gradient was assumed (i.e. behaviour expected for conventional reservoirs (e.g. sandstones)). Ultimately, the $\frac{k_{app}}{k_D}$ ratio will be determined to analyse the Knudsen diffusion and gas slippage effect.

3.2.2 Resolving pressure values

Mass flow is initiated by applied pressure difference on the inlet (p_i) and outlet (p_j) surfaces of the representative cube that contains the pore network. The mass balance at every pore is then applied. The system of equations that results from applying mass balance on every pore is non-linear. To solve for the pressure values, Newton-Raphson iterative method is used;

$$P_{new} = w \times P_{new} + (1 - w) \times P_{old} \tag{11}$$

Where, w is the relaxation factor. The iterative will be stopped when the value of P_{new} has approximately the same value of P_{old}. Having solved for pressures at each pore, the volumetric flux is than evaluated through the entire network and compute apparent permeability K_{app} based on the flux using Darcy's equations that were previously described.

Section IV: Results and Discussion

In this section, sensitivity analysis with different parameters such as pore size distribution and pressure on apparent permeability and Darcy permeability are presented. By determining the ratio of apparent permeability (K_{app})and Darcy permeability (K_D), the slippage and Knudsen diffusion effects on permeability can be analysed and discussed. Additionally, I compare my results with experimental data and existing research [i.e. Mehmani et al 2013; Guo et al. 2013; Sakhaee-Pour and Bryant 2012; Javadpour 2009].

4.1 Pore throat size statistics

Table 1: Pore size statistics used in PoreFlow.

Pore-size statistics	*PORER*	*PORER2*	*PORER4*	*PORER6*	*PORER8*	*PORER10*	*PORER20*
Min pore (r) (mm)	0,3650800 E-5	0.7302900 E-5	0.1459900 E-4	0.2191800 E-4	0.2921200 E-4	0.3651000 E-4	0.7303900 E-4
Max pore (r) (mm)	0.4244700 E-4	8.531500 E-4	0.1750900 E-3	0.2310400 E-3	0.3341300 E-3	0.4241000 E-3	0.8629600 E-3
Mean pore r (nm)	7,936386	15,82027	31,19897	46,39088	65,07642	77,91075	15,73266
Min pipe (r) (mm)	0.3468260 E-5	0.6937755 E-5	0.1386905 E-4	0.2082210 E-4	0.2775140 E-4	0.3468450 E-4	0.6938705 E-4
Max pipe (r) (mm)	0.2255870 E-4	0.5126960 E-4	0.1187595 E-3	0.1513065 E-3	0.3022995 E-3	0.3125975 E-3	0.5553225 E-3
Mean pipe r (nm)	*5,171003*	*10,61086*	*20,96582*	*30,51312*	*42,17162*	*51,87894*	*103,4481*
Min pipe (l) (mm)	0.5075600 E-4	0.6746200 E-4	0.1463050 E-3	0.1913000 E-3	0.2666000 E-3	0.1818700 E-3	0.5381300 E-3
Max pipe (l) (mm)	0.1654244 E-3	0.2803862 E-3	0.5761420 E-3	0.8489076 E-3	0.1152561 E-2	0.1397857 E-2	0.2847025 E-2
Mean pipe (l) (mm)	0.1246919 E-3	0.2076527 E-3	0.1283161 E-3	0.6316029 E-3	0.8568164 E-3	0.1041908 E-2	0.2123611 E-2

Table 1 shows the various pore throat size distribution used for modelling. Note that the throat has to be at least twice the maximum value of the pores for modelling without errors and that the cross sectional area of the pore throats is all circular, considering the SEM images in other literature. Furthermore, a typical shale has characteristic pore throat sizes ranges between 3 nm and 100 nm (Loucks et al. 2012; Curtis et al. 2011; Mehmani et al. 2013). The experimental data were collected from different pore size distribution with an average pore throat diameter of 5, 10, 20, 30, 40, 50 and 100 nm. **Figure 11a-g** shows the histograms of the pore throat size distribution used as parameters for pore network modelling. **Figure 12** is an overview of all the pore throat size distribution.

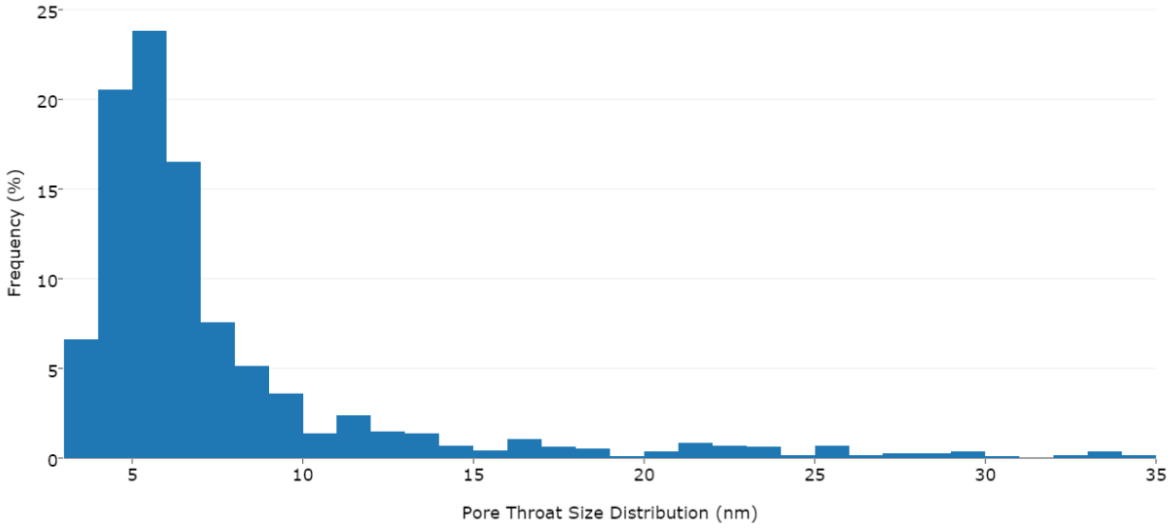

Figure 11a: Histogram of pore throat sizes with r_{avg} = 5 nm

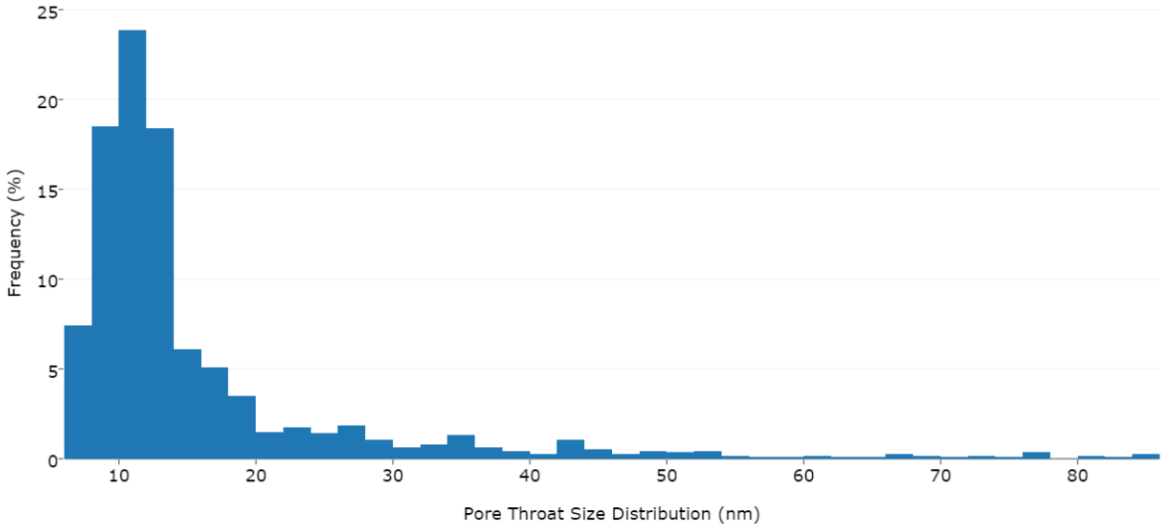

Figure 11b: Histogram of pore throat sizes with r_{avg} = 10 nm

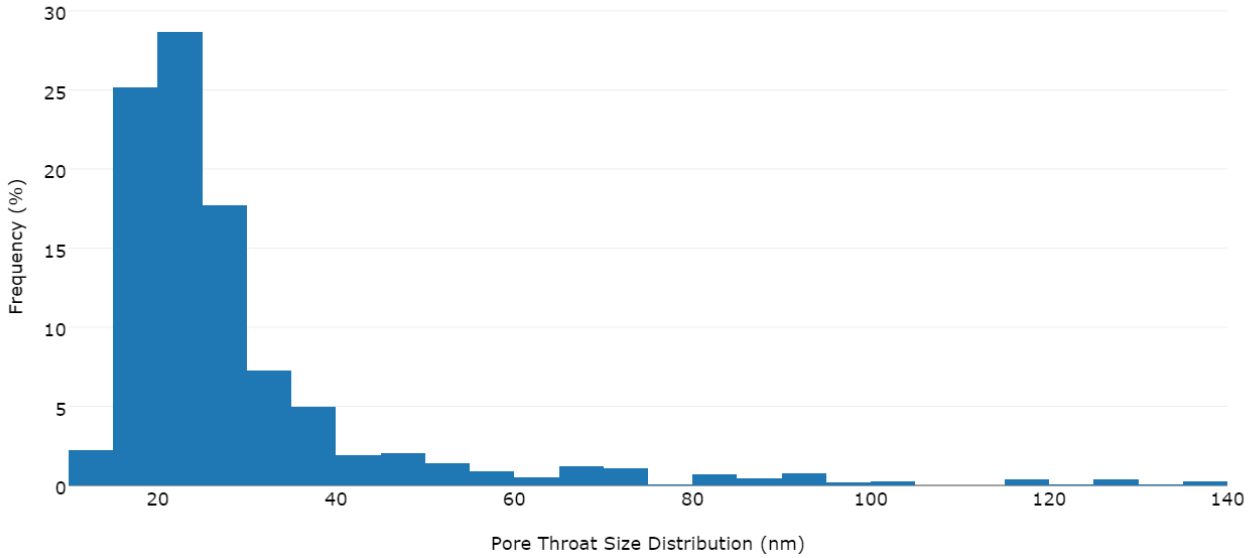

Figure 11c: Histogram of pore throat sizes with r_{avg} = 20 nm

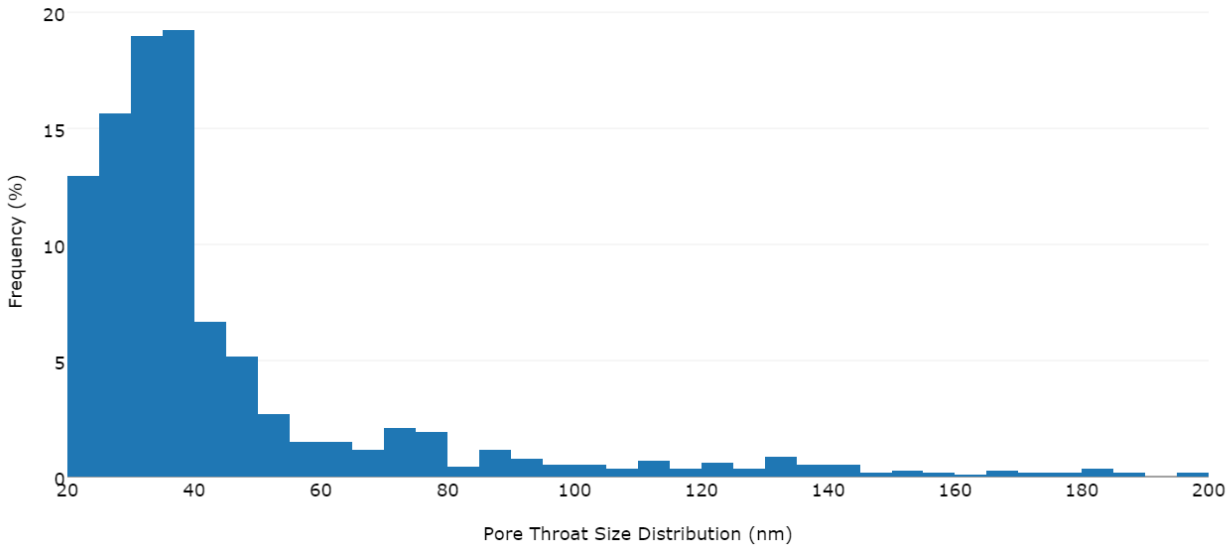

Figure 11d: Histogram of pore throat sizes with r_{avg} = 30 nm

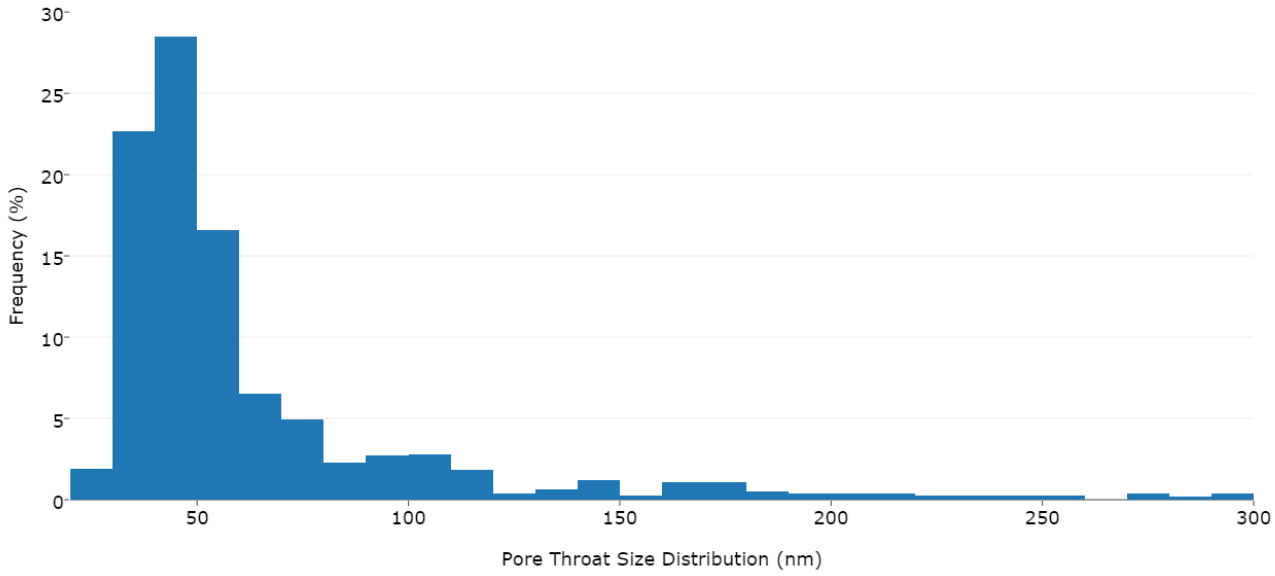

Figure 11e: Histogram of pore throat sizes with r_{avg} = 40 nm

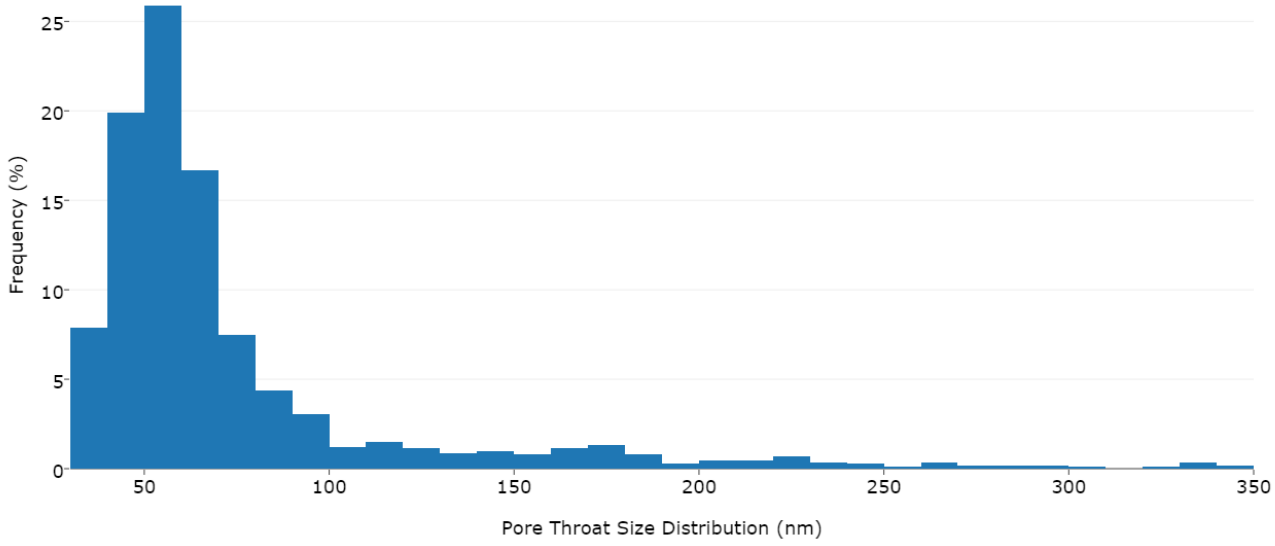

Figure 11f: Histogram of pore throat sizes with r_{avg} = 50 nm

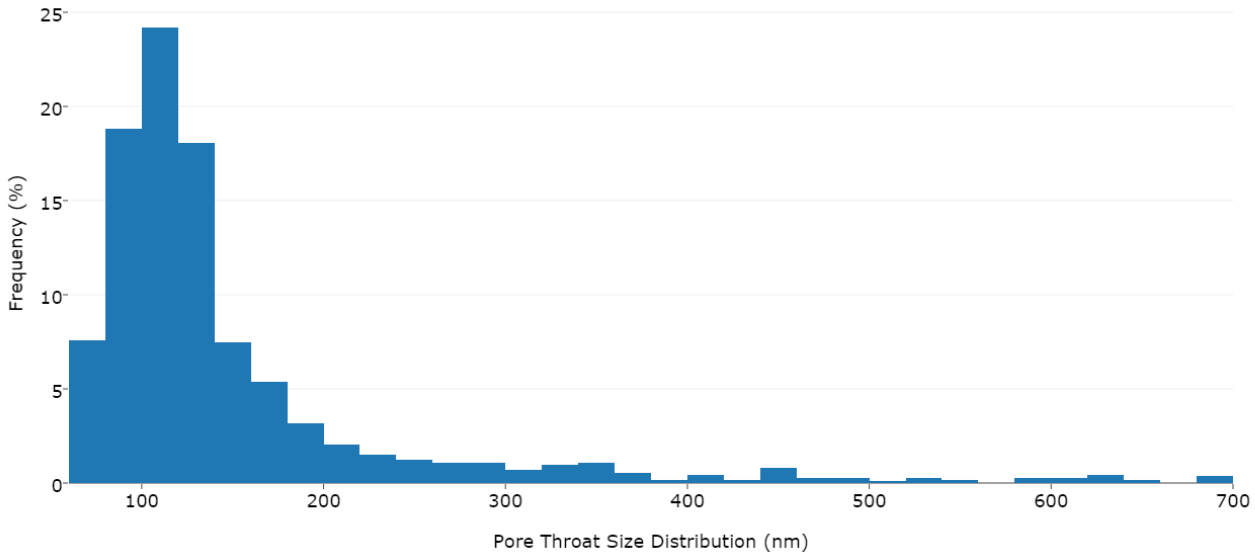

Figure 11g: Histogram of pore throat sizes with r_{avg} = 100 nm

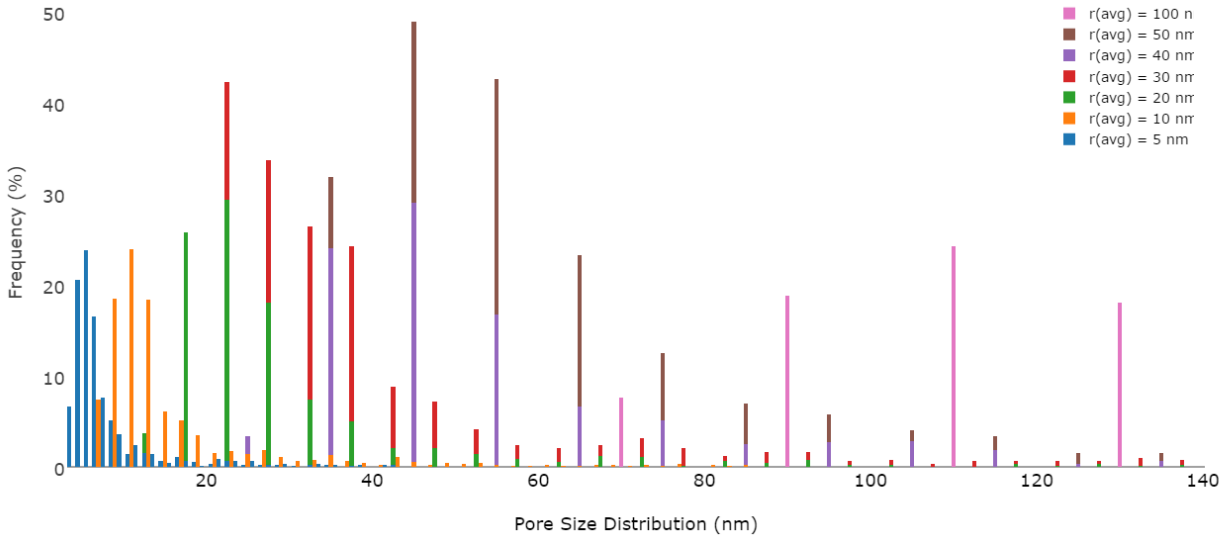

Figure 122: Overview of the pore throat sizes in nm

4.2 Single throat conductance analysis

Before considering the pore network, the effects of Knudsen diffusion and gas slippage on the permeability of a single throat is investigated. Throughout this section, a constant value of viscosity (μ = 1.2 x 10^-5 Pa/s) for methane gas (M = 16.04 kg/kmol) at T=400 K has been used. Viscosity of methane is not strongly dependent on either pressure or temperature for the ranges considered. First, the apparent discharge q_{ij} and Darcy discharge q_D is considered;

$$q_{ij} = \frac{J \times \pi r^2}{\rho} \quad \text{Eq. 1}$$

$$q_D = \frac{\pi r^4}{8\mu} \frac{(\Delta p)}{L} \quad \text{Eq. 2}$$

Where q_{ij} is the volumetric discharge through the pore throat in m^3/s, q_D is the volumetric Darcy discharge through the pore throat in m^3/s, J is the volumetric flux (see eq. 9, section III), *r* is the pore throat radius in m, *L* is the pore throat length in m, Δp is the pressure gradient and ρ is the density in kg/m^3. To investigate the effect of Knudsen diffusion and gas slippage on the apparent permeability of a single pore throat**,** the ratio of apparent permeability k_{app} to Darcy permeability k_D is solved which is equivalent to the ratio of the apparent discharge q_{ij} to Darcy discharge q_D (eq.3). By computing the k_{app}/k_D ratio for various throat radii at various pressures, the effect of gas slippage and Knudsen diffusion can be analysed in **figure 13**.

$$\frac{q_{ij}}{q_D} = \frac{k_{app}}{k_D} \quad \text{Eq. 3}$$

$$\frac{k_{app}}{k_D} = \frac{2\mu M}{3\times 10^3 RT\rho}\left(\frac{8RT}{\pi M}\right)^{0.5}\frac{8}{r} + \left[1 + \left(\frac{8\pi RT}{M}\right)^{0.5}\frac{\mu}{pr}\left(\frac{2}{\alpha} - 1\right)\right]\frac{1}{\rho} \quad \text{Eq. 4}$$

Where *M* is the molar mass in kg/kmol, *T* is the temperature in K, *R* is the gas constant in J/mol/K, μ is the viscosity in Pa/s, ρ is the density in kg/m^3 , *p* is the pressure in kPa and α = tangential accommodation coefficient.

Table 2: Ratio of k_{app}/k_D at a single throat (r) at various pressures.

Throat radius (m)	Pressures (kPa)	Kapp/Kd (fixed 5nm)	Kapp/Kd (fixed 10nm)	Kapp/Kd (fixed 20 nm)	Kapp/Kd (fixed 30 nm)	Kapp/Kd (fixed 50 nm)	Kapp/Kd (fixed 100 nm)
5 E-09	**1000**	400,8636758	201,194033	101,3592116	68,08093784	41,4583188	21,49135452
10 E-09	**5000**	84,02999962	42,777212	22,15080112	15,27533083	9,774954595	5,649672419
20 E-09	**10000**	44,42581143	22,97510937	12,24974981	8,674629952	5,814534069	3,669462156
30 E-09	**20000**	24,62371733	13,07405805	7,299224149	5,374279514	3,834323806	2,679357025
40 E-09	**30000**	18,0230193	9,773707616	5,64904893	4,274162701	3,174253718	2,349321981
50 E-09	**50000**	12,74246087	7,133427265	4,328908755	3,394069251	2,646197648	2,085293946
100 E-09	**100000**	8,782043761	5,153217002	3,338803623	2,733999163	2,250155596	1,88727292

Table 3: Base case input parameters for single throat analysis (methane gas)

Input Data	*Value*
Molar mass (g/mol)	16,04
Density $\boldsymbol{\rho}$ (kg/m3)	0,656
Viscosity $\boldsymbol{\mu}$ (Pa/s)	0,000012
Gas Constant R (J/K/mol)	8,314
Temperature T (Kelvin)	400
$\boldsymbol{\alpha}$	0,8

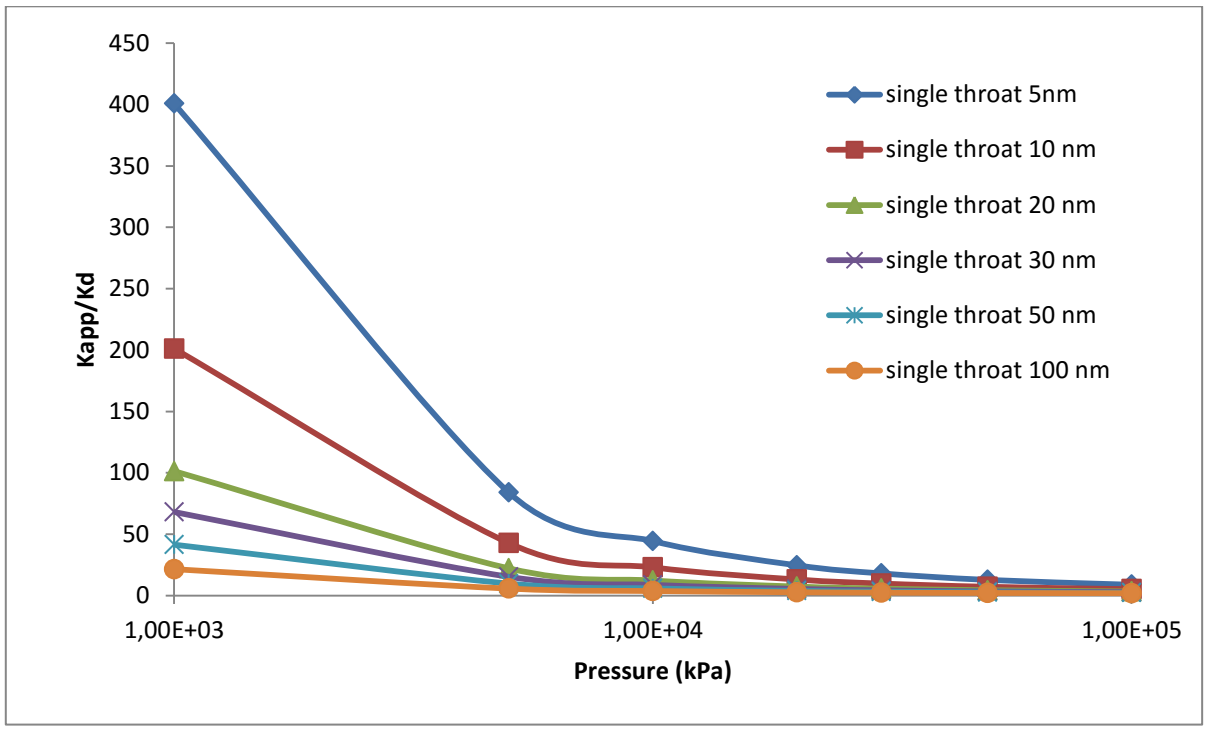

Figure 13: Effect of pressure on gas permeability in single pore throats. The following parameters for methane gas has been used throughout the section; M = 16.04 , T = 400 K, R = 8.314, ρ = 0.656 with various pressure and pore throat radii.

These results show that the k_{app}/k_D ratio is sensitive to pressure and, at lower pressures, the mean free path of the gas molecules increases as does deviation from Darcy flow. The gas permeability is greater than the reference (Darcy) permeability for all throats, with the effect being greater in narrower throats (i.e. r < 10 nm). Furthermore, throat sizes larger than 100 nm show almost no difference between apparent permeabilities and Darcy permeabilities. As throat sizes decrease, the Knudsen diffusion and gas slippage become dominant, leading to an increase in apparent permeability. The highest contribution of the Knudsen diffusion effect is reached for pores in the range of 5 – 10 nm. Similar dependencies on pressure and throat size have also been computed by authors like Javadpour (2007) where the apparent permeability of as single channel is also considered, or a combination of pores with nanometre and micrometre sizes with different flow physics mechanisms on both scales (Mehmani 2013). Although the experimental data in this research may slightly differ from others, i.e. higher k_{app} / k_D values for different single pore throat sizes, it still clearly show the effect of pressure and the pore throat size on k_{app}/k_D ratio.

For a typical shale sample (e.g. Barnett), the characteristic throat size of 6 nm corresponds to the largest fraction of conduits (Sakhaee-Pour and Bryant, 2012). The pore size distribution seen in histogram 11a will be most likely similar to a typical shale sample.

Figure 14 shows the effects of gas molar mass on the k_{app}/k_D ratio. The gas molar mass has only a minimal effect on the ratio, with a slight increase at lower molar mass values. The amount of pressure still has a bigger impact.

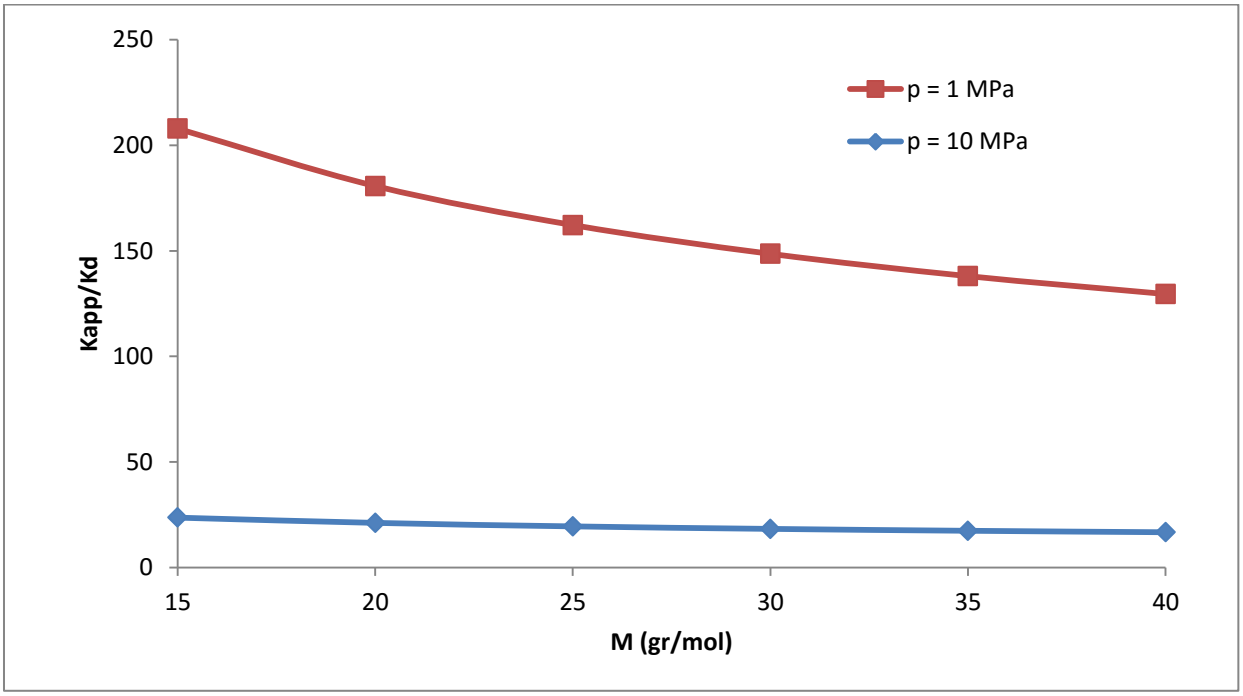

Figure 14: Effects of molar mass on the k_{app}/k_D ratio. Pore throat radius = 10 nm, T = 400 K.

4.3 Network throat conductance analysis

A regular cubic lattice network is used to model the gas flow through a pore network similar to a shale gas reservoir. Seven different pore throat size distributions in the range of 3 – 100 nm are compared at different pressures in the inlet and outlet of the pore throat network (ranging from 1 MPa to 100 MPa). After having solved for the pressures values at each pore and evaluating the volumetric flux *q* through the entire network, apparent permeability can be computed;

$$k_{app} = \frac{q\mu L}{A\Delta P} \qquad \text{Eq.5}$$

Here, the cross-sectional area *A*, L, length *L* and pressure difference ΔP refer to the entire network. The ratio k_{app}/k_D can then be calculated and plotted using the PoreFlow model. **Figure 15** shows a schematic of an example of a pore throat network. An amount of pressure at inlet pushes the flow towards the pressure outlet with a pressure gradient of 10 kPa. **Figure 16** shows the effect of pressure on conductivity whereas **figures 18 – 20** shows the effect of pore throat sizes on conductivity.

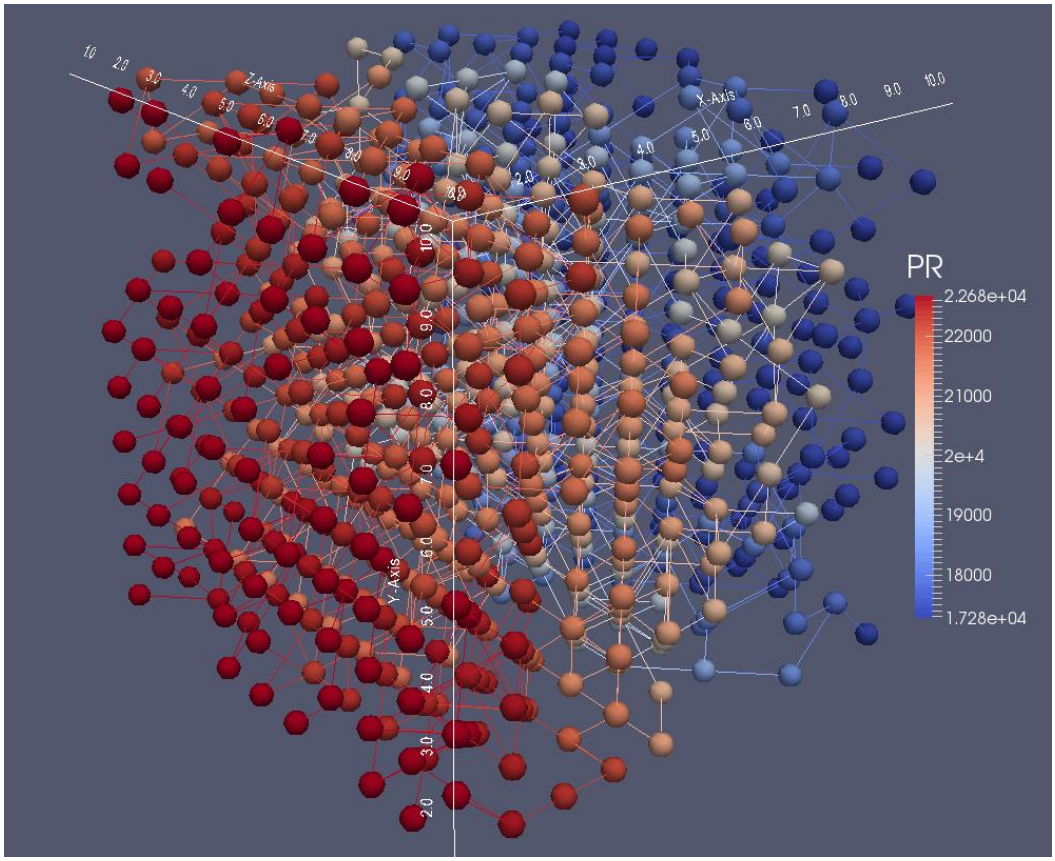

Figure 15: Schematic of the pore throat network. Each sample used for modelling consists between 1133 and 1147 throats.

Table 4: Ratio of Kapp/Kd at various pore throat sizes (r) at various pressures in a network using PoreFlow model.

Pressure (MPa)	*Kapp/Kd with r_{avg} = 5 nm*	*r_{avg} = 10 nm*	*r_{avg} = 20 nm*	*r_{avg} = 30 nm*	*r_{avg} = 40 nm*	*r_{avg} = 50 nm*	*r_{avg} = 100 nm*
100	4,2999	2,6554	1,8241	1,5464	1,4179	1,3346	1,1598
50	6,844	3,9287	2,4589	1,967	1,7396	1,5927	1,283
30	8,1162	5,6242	3,3038	2,564	2,1673	1,9362	1,4468
28	10,841	5,9269	3,4546	2,6262	2,2436	1,9975	1,476
20	14,474	7,7421	4,359	3,2245	2,7009	2,3649	1,651
10	27,187	14,093	7,5218	5,3158	4,2982	3,6491	2,2617
5	52,612	26,791	13,844	9,4941	7,488	6,2141	3,4788
1	256,01	128,37	64,412	42,903	32,983	26,718	13,186

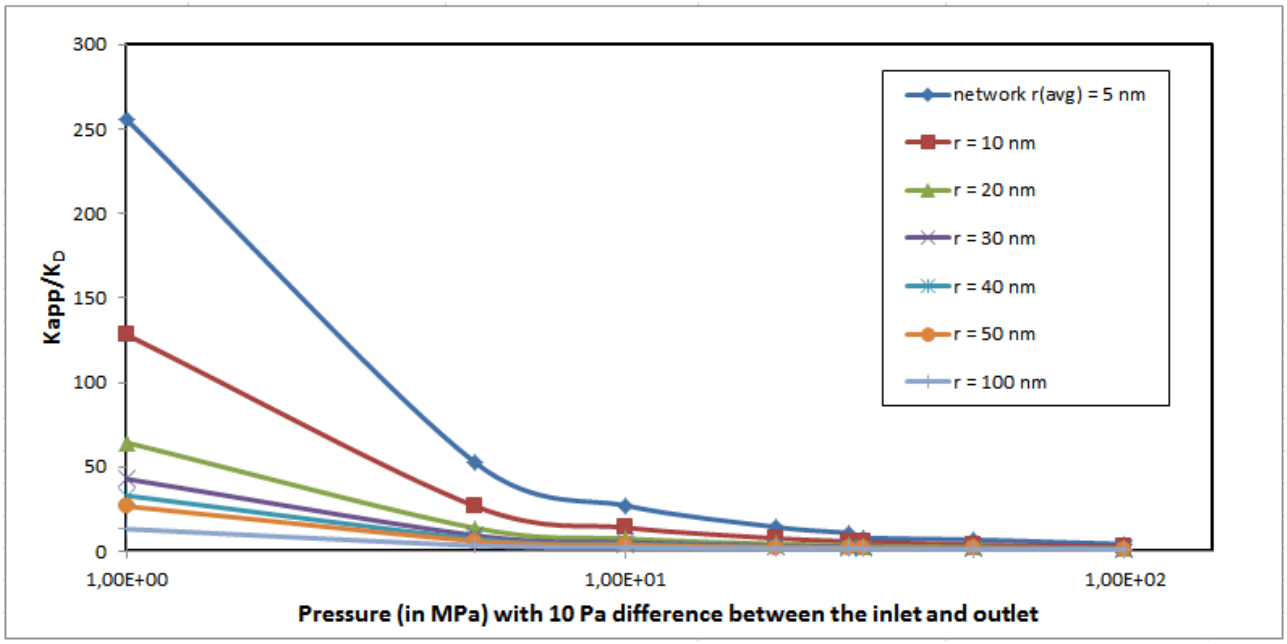

Figure 16: Effect of pressure on gas conductivity. The network has an average throat radii of 5, 10, 20, 30, 40, 50 and 100 nm.

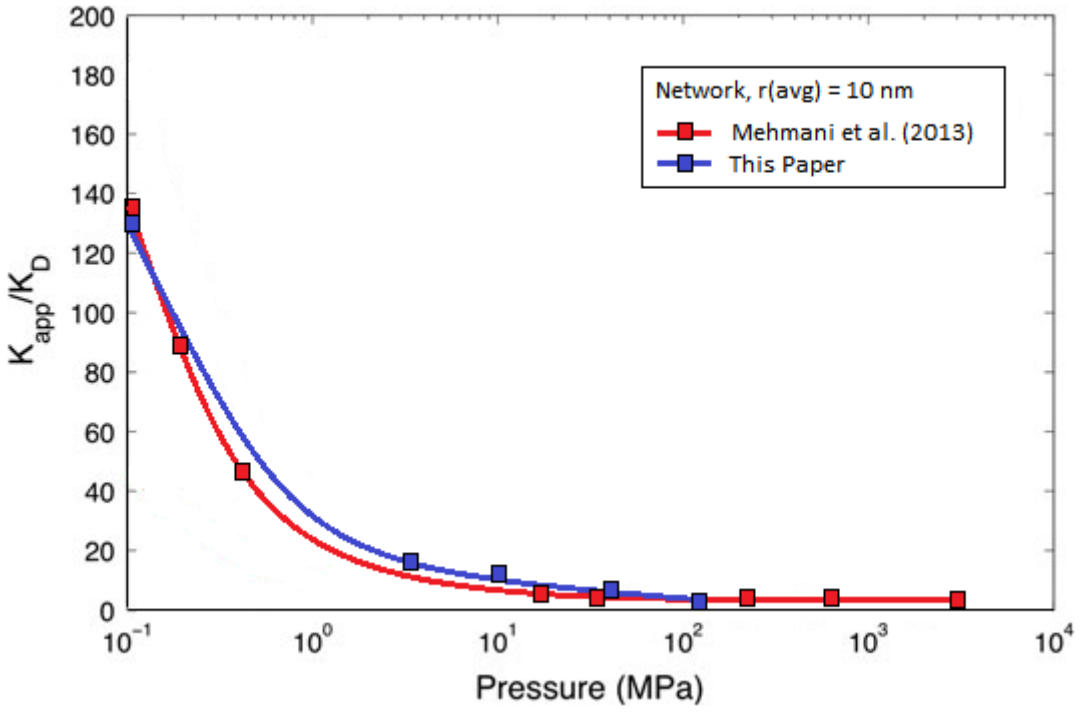

Figure 17: Comparison of k_{app}/k_d ratio in a pore throat network, Mehmani et al. (2013) and experimental data.

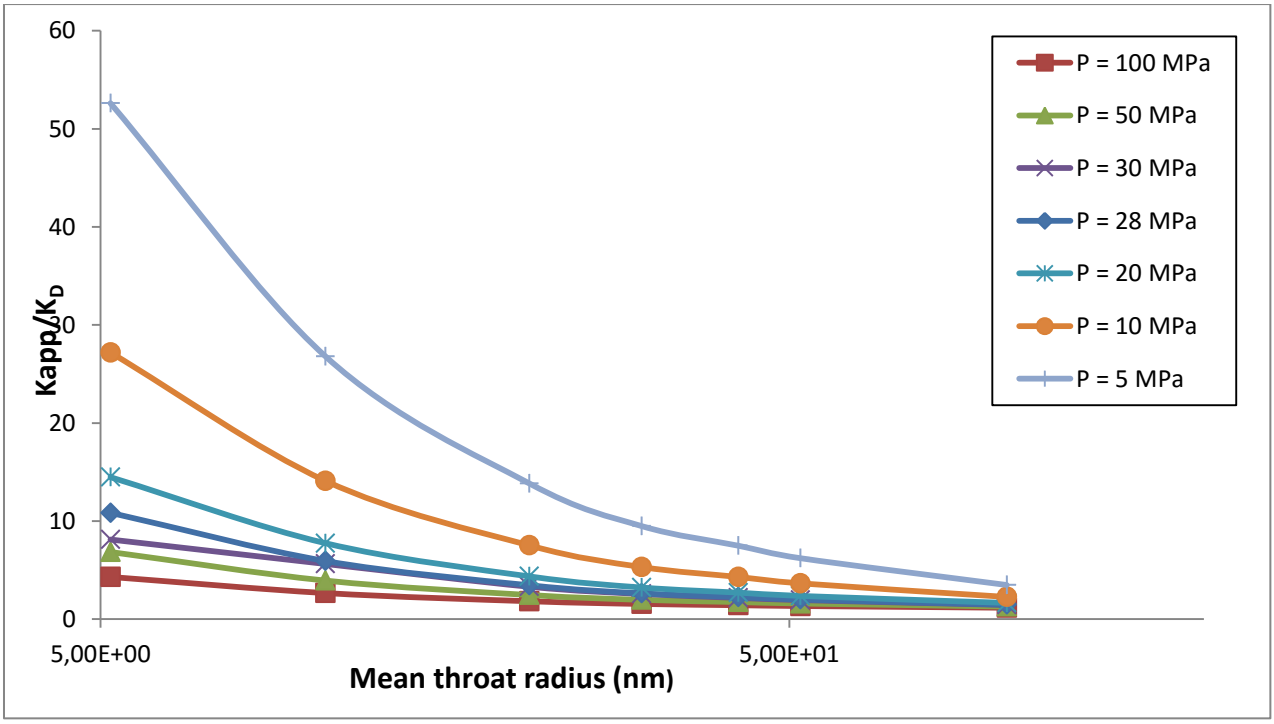

Figure 18: Effect on pore throat sizes (mean pipe (r)) on conductivity with various pressure values.

With a constant pore throat radius of 5 nm, the K_{app}/K_d ratio at 5 MPa is 84 while the K_{app}/K_d ratio at 50 MPa is 13 (**fig. 16**). Thus, results show one to two order of magnitude change in permeability and explain the unusual gas production from shale rock compared with conventional gas production. It also illustrates that Knudsen diffusion and gas slippage close to the boundaries become prominent at low pressures (e.g. 5 and 10 MPa) causing significant increase in permeability. This fits with the experimental data of Mehmani et al. (2013) (**fig. 17**). It also suggest that the smaller the pore throat sizes, the larger the ratio between apparent permeability and Darcy permeability become. So, the deviation between apparent permeability and Darcy permeability is larger at lower pressures. Moreover, the contribution of Knudsen diffusion to total gas flow is larger at lower pressures. **Figure 18** shows the effect on pore throat sizes on gas permeability with various pressure values. An increase in the ratio is expected in the nanometre range. This is also due to processes of gas slippage and Knudsen diffusion which significantly influences the gas flow transport at (nano)pore-scale. Note that the pore throat sizes at micro-scale (i.e. r > 1 μm) become irrelevant to the gas flow permeability that is controlled by the pore throats (**fig. 19**). In the absence of desorption, pore sizes are immaterial to calculate gas permeability. In addition, the contribution of Knudsen diffusion is almost negligible for pores larger than 1 μm which is the reason that, in conventional systems, Knudsen diffusion is not included in conventional gas flow models.

Sakhaee and Bryant (2012) mentioned an initial pressure of a typical shale gas reservoir at the inlet of the pore network structure to be 28 MPa where the effect of pressure on gas slippage is accounted for. PoreFlow network modelling suggest that, with an average pore throat size of 10 nm in a pore network, the apparent permeability of 4.5268 10^{-15} m^2 at the start of production (Pressure at the inlet is 28 MPa) is significantly smaller than at the late production(i.e. pressure at the inlet is 10 MPa) where the apparent permeability is increased to 2.0463 10^{-14} m^2. Reason for this effect of the declining field pressure on the gas permeability using the network model is the adsorbed layer. Proven that with smaller amount of pressure at the inlet, the apparent permeability of the shale gas reservoir increases. More so, the gas flow is initiated by applied pressure difference on the inlet (p_i) and outlet (p_j) and must be solved for pressure values at each pore using the Newton-Raphson iterative method. But, unlike flow in conventional reservoirs, gas permeability in shale gas also depend on the absolute pressure values in individual pores. Specifically, smaller pressures result in an increase in permeability.

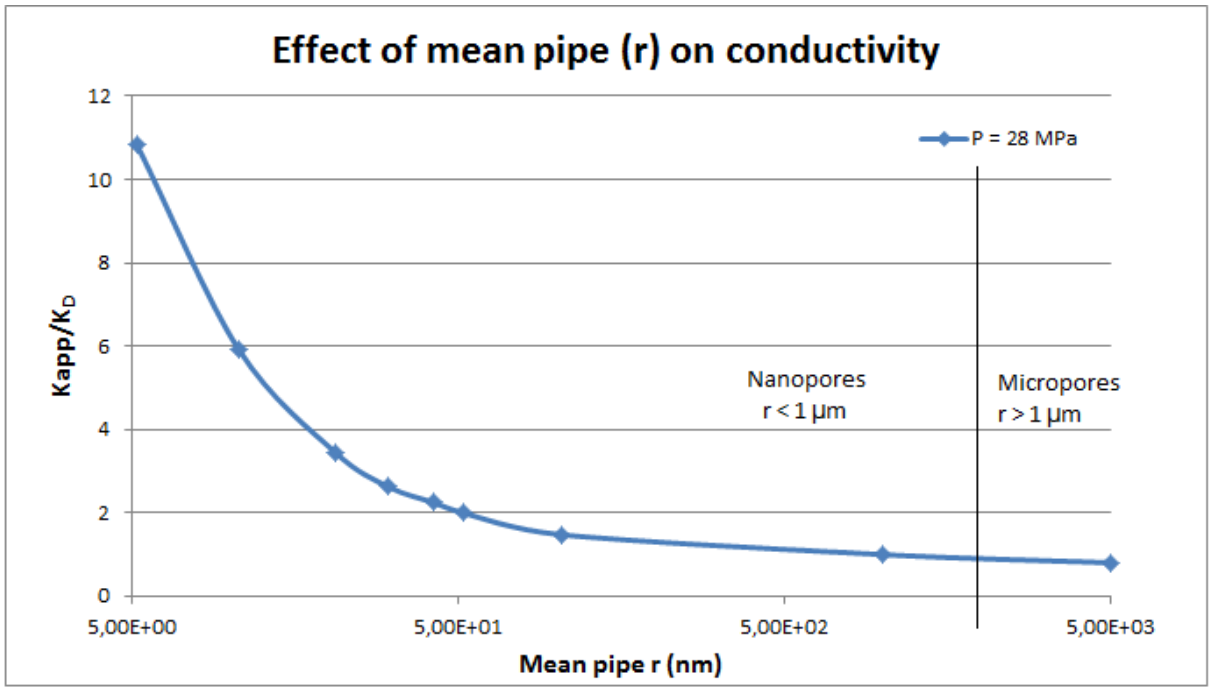

Figure 19: Effect of pore size on the ratio showing a difference between nano and macropores.

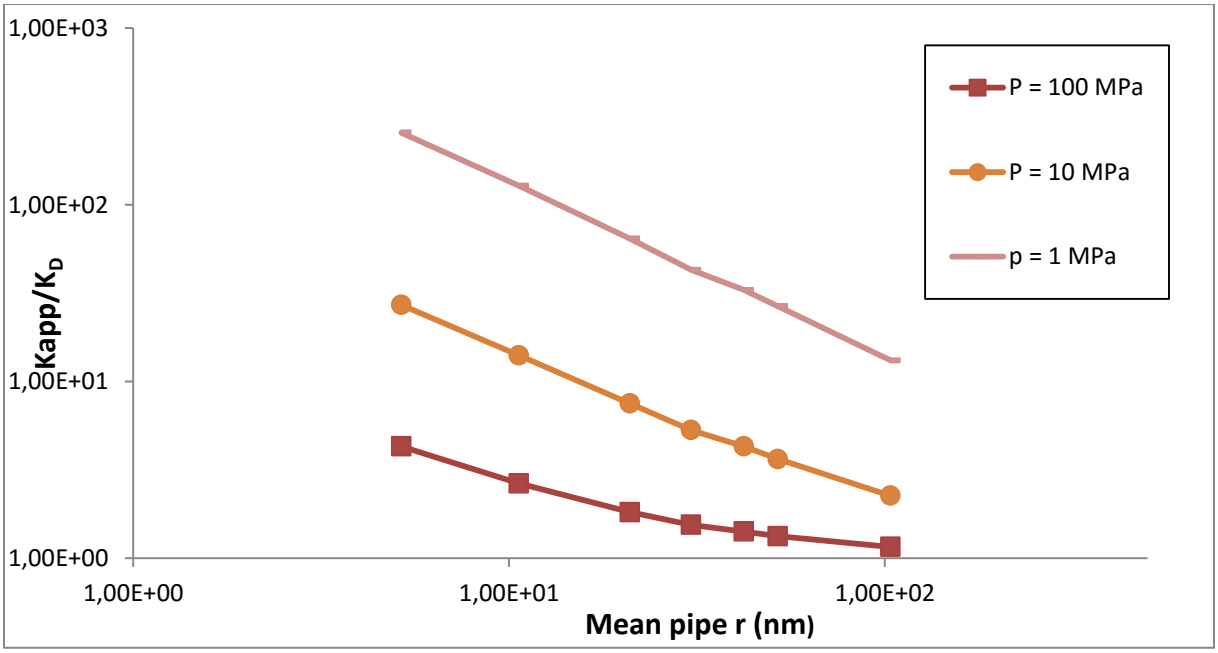

Figure 20: Effect of throat sizes and pressure on normalized Kapp/Kd in multi-directional pore scale network.

Furthermore, the values of average as density, viscosity and slip coefficient are pressure dependent, and therefore the apparent permeability is also pressure dependent. The Knudsen diffusion contribution to total flow gets relativity smaller than the slip flow contribution. In addition to Knudsen diffusion and slip flow, configurational diffusion and surface diffusion may also contribute to the overall gas flow in nanopores (Darabi et al. 2012).

Figure 20 demonstrates the behaviour of normalized gas permeability in a multi-directional pore scale network versus the throat size for 1, 10 and 100 MPa respectively and shows a linearly dependency. The apparent permeability has a strong dependence on pressure, i.e. curves for different pressures are much further apart. Mehmani et al. (2013) mentioned that as the main radius decreases, gas slippage on gas conductivity increases the apparent permeability. This makes the effective slope less and less steep as seen in **figure 20**, especially at higher pressures. More so, if pressure falls below the critical desorption pressure in shale systems, gas molecules detach from the pore walls in organic matter, consequently enlarging the pores and improving permeability (Naraghi and Javadpour, 2015).

Summary and Conclusion

This master's thesis presents a pore scale modelling study gas flow and transport in low permeability rock (e.g. shales). Pore network analysis with different parameters such as pore throat sizes, pressure and gas molar mass on apparent permeability are presented. The challenge is to model the coupling of gas flow and transport simulations involving different physics at different scales encountered in porous media. Furthermore, gas permeability of shale is affected significantly by gas slippage on the pore walls and Knudsen diffusion. These processes can be neglected for larger pores (i.e. $r > 1$ µm) but begins to play a considerable role in smaller nanopores. Literature on shale gas flow and transport show that the behaviour of gas transport in porous media can be characterized into different flow regimes, i.e. continuum, slip, transition and free molecular flow regime. Gas transport in a tight reservoir (e.g. shales) show that the slip and transition flow regime are the most dominant. This because neither the Knudsen diffusion nor viscous flow can be ignored in these regimes due to the variety in pores ranging from nano-to micrometre. A newly developed pore network model called PoreFlow is used to simulate gas flow and used for upscaling flow and transport in porous media to see how different pore scale processes manifest themselves at continuum scales. Shale gas flow and transport in individual pore throats and in pore throat networks is evaluated where very small throat sizes are distributed randomly in the network. We use complex formulations for more accurate modelling of transport problems in presence of the non-wetting phase which is done by refining the discretization within drained pores and calculating dissolved solute and adsorbed mass concentrations in edges of drained pore bodies and pore throats. During modelling at every stage of the process, non-wetting phase (in this case gas) invades all accessible pore bodies and throats with the lowest entry capillary pressure. An overall mass flux equation for gas flow in a cylindrical tube is used that is governed by a combination of Knudsen diffusion and gas flow due to pressure forces. This was proposed by Javadpour (2009) introducing the concept of apparent permeability. Pore throat size distribution with average pore throat sizes of 5, 10, 20, 30, 40, 50 and 100 nm has been used for modelling.

Numerical results of gas transport in single pore throats show significant difference in the permeability due to absolute pressure difference and the pore throat sizes. With a constant pore throat radius of 5 nm, a K_{app}/K_d ratio at 5 MPa is 84 while a pressure 10 times bigger (50 MPa) shows a K_{app}/K_d ratio of 13. Thus, results show one to two order of magnitude change in permeability and explain the unusual gas production from shale rock compared with conventional gas production . Pores as small as 1 µm show no difference between apparent permeability and Darcy permeabilities. Pressures as small as 1 MPa shows a K_{app}/K_d ratio is between 150-200 whether at a higher pressure of 10 MPa shows a constant ratio meaning that the effect of Molar mass does not influence that much on the permeability of rock. Results of the pore throat network modelling show that, at small pore throat scales (e.g. 5, 10, 20 and 30 nm), the K_{app}/K_d ratio increases significantly towards smaller pressures. Results with an average pore throat distribution size of 20 nm in a pore network, show a strong correlation with data obtained by Mehmani et al. (2013).

The initial pressure of a typical shale gas reservoir at the inlet of the pore network structure is 28 MPa (Sakhaee and Bryant, (2012) where we account for the effect of pressure on gas slippage. Network modelling suggest that, with a mean pore throat size of 10 nm in a pore network, the apparent permeability of $4.5268\ 10^{-15}$ m^2 at the start of production (Pressure at the inlet is 28 MPa) is

significantly smaller than late production(i.e. pressure at the inlet is 10 MPa) where the apparent permeability is increased to 2.0463 10^{-14} m^2. Reason for this effect of the declining field pressure on the gas permeability using the network model is the adsorbed layer. Proven that with smaller amount of pressure at the inlet, the apparent permeability of the shale gas reservoir increases. Moreover, the gas permeability in shale gas highly depends on not only the pressure gradient (Δp) but also the amount of pressure, unlike conventional reservoirs. This has major implications in shale gas reservoir simulations and models. So, in terms of shale gas production, gas slippage and Knudsen diffusion dominates at smaller pressures typical of those after longer periods of production. As consequence of shale gas production and consequently pressure decline, the reservoir matrix permeability is predicted to increase through the life of a well. Additionally, bigger pore throat sizes (µm-mm) are the main permeable channels in shale gas reservoirs. These high pore throat radii can be seen as shale fractures and have a great impact on the gas production of shale gas reservoirs. Darcy's law is suitable for gas flow through these fracture channels.

To summarize;

1. Pore throat size distribution at nano-scale in shale gas formations strongly contribute to the gas flow process through the network and significantly affect gas permeability. Gas flow in nano-pores deviate from the traditional flow models used for conventional reservoirs containing larger pore sizes using e.g. Darcy's equation or Fick's law. The contribution of Knudsen diffusion is negligible for pores larger than 1 µm which is the reason that, in conventional systems, Knudsen diffusion is not included in flow models.
2. Gas transport through large fraction of nanopores result in higher apparent permeability compared with its intrinsic permeability. The results clearly show that the apparent permeability to Darcy permeability ratio is higher at smaller pores and lower pressures. To be more precise, the effect of Knudsen diffusion and gas slippage on gas permeability is higher in smaller pores (i.e. r <20 nm)and at lower pressures (i.e. p <20 MPa). Gas slippage has the primary effect at small pressures (p = 5 MPa - 10 MPa) and the highest contribution of the Knudsen diffusion effect is reached for pores in the range of 5 – 10 nm. Temperature and molar mass have only minimal effects on the pore throat structure.
3. Because of the small pore size, capillary forces can dominate fluid transport in shale gas reservoirs. Although the pressure gradient drive the flow of gas, gas permeability in shale gas also depends on absolute pressure values in individual pores. Specifically, smaller pressures result in an increase in permeability.
4. For complete validation of the PoreFlow model, measurements with similar pressures and pore throat diameters have been conducted and the model was found to match very well with the experimental data found in literature (e.g. Mehmani et al. 2013; Javadpour, 2009).

Finally, additional research on shale gas flow in tight reservoirs is necessary. At the moment there is no uniform equation for describing gas transport through tight reservoirs. More conducting research in the complex transport equations with transport mechanisms appropriate for shale gas reservoirs is necessary. Also, research on the relationship of shale porosity and permeability trends may need more attention.

References

Akkutlu I.Y., Fathi E. 2012; *Multiscale gas transport in shales with local kerogen hetero geneities.* SPE 17, pp. 1002-1011.

Amann-Hildenbrand A., Ghanizadeh A., Krooss B.H. (2012); Transport properties of unconventional gas systems. Marine and Petroleum Geology 31 (2012) 90-99

Ayala H.L.F., Ertekin T., Dewumi M. (2007); *Numerical analysis of multi-mechanistic flow effects in naturally fractured gas-condensate systems*. J. Pet. Sci. Eng., Vol 58, pp. 13-29

Barisik and Beskok (2014); *Scale effects in gas nano flows*. Physics of Fluids 26 (2014), Issue 5

Beskok A., Karniadakis G.E. (1999); *Report: A model for flows in channels, pipes and ducts at micro and nano scales.* Microscale Thermophys. Eng. 3 (1), 43-77

Bhatia S.K. and Nickelson D. (2010); *Some pitfalls in the use of the Knudsen equation in modelling diffusion in nanoporous materials*. Chemical Engineering Science 66 (2011) 284-293

Bird R.B., Stewart W.E., Lightfoot E.N. (2007); *Transport phenomena*. Second Edition, John Wiley & Sons, Inc, Hoboken NY (2007)

Blunt M.J. (2001); *Flow in porous media – pore-network models and multiphase flow*. Current Opinion in Coll. & Interf. Sc. 6.

Blunt M.J., Bijelijic B., Dong H., Gharbi O., Iglauer S., Mostaghimi P., Paluszny A., Pentland C. (2013); *Pore-scale imaging and modelling*. Advances in Water Resources 51, 197-216.

Bravo, M.C. (2007); *Effect of transition from slip to free molecular flow on gas transport in porous media*. Journal of Applied Phys. 102.

Brown G.P., DiNardo A., Cheng G.K., Sherwood T.K. (1946); *The flow of gases in pipes at low pressure*s. Journal of Applied Phys., Vol 17, 802-813

Bustin A.M.M., Bustin R.M (2012); *Importance of rock properties on the producibility of gas shales*. Intern. J. of Coal Geology 103, pp. 132-417

Cai Q., Buts A., Seaton A., Biggs M.J. (2008); *A pore network model for diffusion in nanoporous carbons: Validation by molecular dynamics simulation*. Chemical Engineering Science 63 (2008) 3319-3327

Curtis M.E., Ambrose R.J., Sondergeld C.H., Rai C.S. (2011): *Investigation of the relationship between organic porosity and thermal maturity in the Marcellus Shale.* SPE paper 144370 presented at SPE North American Unconventional Gas Conference and Exhibition, The Woodlands.

Chen C., Hu D., Westacott D., Loveless D. (2013); *Nanometer-scale characterization of microscopic pores in shale kerogen by image analysis and pore-scale modelling.* Geochemistry Geophyiscs Geosystems, Volume 14 number 10, 4066-4075.

Civan F. (2010); *Effective correlation of apparent gas permeability in tight porous media.* Transp. Porous Media 82, pp. 375-384.

Civan F., Rai. C.S., Sondergeld C.H. (2011); *Shale-gas permeability and diffusivity inferred by improved formulation of relevant retention and transport mechanisms*. Transp. Porous Med. 56, pp. 925-944

Dewers T.A., Heath J., Ewy R., Duranti L. (2012); *Three-dimensional pore networks and transport properties of a shale gas formation determined from focused ion beam serial imaging*. Int. J. Oil, Gas and Coal Technology, Vol 5, pp. 229-248

Ding W., Li H., Pfeifer P., Dittmeyer R. (2014); *Crystallite-pore network model of transport and reaction of multicomponent gas mixtures in polycrystalline microporous media*. Chemical Engineering Journal 254 (2014) 545-558

Fathi E., Tinni A., Akkutlu Y. (2012); *Correction to Klinkenberg slip theory for gas flow in nano-capillaries*. Intern. J. of Coal Technology, Vol 103, pp. 51-59.

Fatt I. (1956b); *The network model of porous media. II. Dynamic properties of a single size tube network*. Trans AIME 207 (1956b) 160-163

Fiedler T., Belova L.V., Murch G.E. (2011). *Numerical simulation of Knudsen diffusion in metallic foam*. Computational Materials Science 50 (2011) 1795-1799

Florence F.A., Rushing J.A., Newsham K.E., Blasingame T.A. (2007); *Improved permeability relations for low-permeability sands*. SPE 107954, presented at the SPE Rocky Mountain Oil & Gas Techn. Symp. 2007

Freeman C.M., Moridis G.J., Blasingame T.A. (2011*); A numerical study of microscale flow behaviour in tight gas and shale gas reservoir systems*. Transport Porous Media 90 (2011) 253-268

Guo C., Xu J., Wu K., Wei M, Liu S. (2015); *Study on gas flow through nano pores of shale gas reservoirs*. Fuel 143 (2015) 107-117

Hassan H.M.H. Way D. (1996); *Gas transport in microporous silica membrane*. SPE paper 36226 presented at the SPE Abu Dhabi Intern. Petrol. Exhib. And Confer. (1996)

Javadpour F., Fisher D., Unsworth M. (2007); *Nanoscale gas flow in shale sediments.* Journal of Canadian Petroleum Tech. Vol. 46, pp. 55-61

Javadpour F. (2009); *Nanopores and apparent permeability of gas flow in Mudrocks (shales and siltstone)*. J. Can. Petroleum Technology 48 (2009) 16-21

Joekar-Niasar, V. Hassanizadeh S.M. (2012); *Analysis of fundamentals of two-phase flow in porous media using dynamic pore-network models: A review*. Critical Reviews in Environ. Sc. And Tech., Vol 52, pp. 1895-1976

Jun Y., Hai S.,Dong-yan F., Chen-chen W., Zhi-xue S.(2013); *Numerical simulation of gas transport mechanisms in tight shale gas reservoirs*. Petroleum Science, December 2013, Volume 10, Issue 4, pp 528-537

Karniadakis G., Beskok A., Aluru N. (2005); *Microflows and nanoflows: Fundamentals and Simulation*. Springer Scienc+Buisness Media INc., NY (2005)

Klinkenberg L.J. (1941); *The Permeability of porous mediato liquids and gases.* American Petroleum Institute, Drilling and Production practice, NY, pp 200-213.

Knudsen M. (1909); Die gesetze der molekularströmung und der inneren reibungsströmung der gase durch röhren. Ann. Phys., Vol 133, pp. 75-130

Kuila U., Prasad M., Kazemi H. (2013); *Assessing Knudsen flow in gas-flow models of shale reservoirs*. CSEG Recorder, May 2013, Vol. 35 No. 05

Laudone G.M., Matthews G.P., Gane P.A.C. (2008); *Modelling diffusion from simulated porous structures*. Chemical Engineering Sciences 63 (2008) 1987-1996

Liu W., Jiang P., Xiang H. (2012); *Experimental and molecular dynamics study of gas flow characteristics in nanopores*. Computational Physics 57 (2012) 1488-1493

Loucks R., Reed R., Ruppel S.C., Hammes U. (2012): *Spectrum of pore types and networks in mudrocks and a descriptive classification for matrix-related mudrock pores*. AAPG Bull. 6, 1071-1098

Mason E.A., Malinauskas A.P. (1983); *Gas transport in porous media: The Dusty-gas model*. Chem. Eng. Mongographs, Elsevier Science (1983)

Maxwell J.C. (1995); *The scientific Letters and Papers of James Clerk Maxwell, Vol. II: 1862-1973*. Harmon, P.M., Cambridge University Press, UK, 1995

Mehmani A., Prodanovic M., Javadpour F. (2013); *Multiscale, Multiphysics Network Modeling of Shale Matrix Gas Flows*. Transport in Porous Media, September 2013, Volume 99, Issue 2, pp 377-390

Naraghi M.E. and Javadpour F. (2015); *A stochastic permeability model for the shale-gas systems*. International Journal of Coal Geology 140 (2015) 111-124

Nelson P.H (2009); *Pore-throat sizes in sandstones, tight sandstones, and shales*. AAPG Bulletin Volume 93, Issue 3, March 2009, pp 329-340

Peng S., Zhang T., Ruppel S.C. (2014); *Upscaling of pore network and permeability from micron to millimetre scale in organic-pore dominated mudstones*. AAPG Annual Convention and Exhibition (2014)

Polczer S. (2009); *Shale to supply half of North America's gas*. Calgary Herald

Raoof A. (2011*); Reactive/Adsorptive Transport in (Partially-) Saturated Porous Media; from pore scale to core scale*. Environmental Hydrology Group PhD, Utrecht University Repositiory (Dissertation)

Raoof A., Nick H.M., Hassanizadeh S.M., Spiers C.J. (2013); *PoreFlow: A complex pore-network model for simulation of transport in variably saturated porous media*. Computers & Geosciences 61 (2013), pp. 160-174

Ren J., Guo P., Guo Z., Wang Z. (2015); *A lattice boltzmann model for simulating gas flow in kerogen pores*. Transp. Porous Med. 106 (2015) 285-301

Roy S., Raju R., Chuang H.F., Cruden B.A., Meyyappan M. (2003); *Modeling gas flow through microchannels and nanopores.* Journal of Applied Physics, Volume 93, Number 8, pp 4870 -4879

Sahimi M. and Tsotsis T.T. (2003); *Molecular pore network models of nanoporous materials*. Phsysica B 338 (2003) 291-297

Sakhaee-Pour A., Bryant S.L. (2012); *Gas permeability of shale (SPE 146944)*. SPE Reservoir Evaluation & Engineering August 2012, 401-409.

Sakhaee-Pour A., Bryant S.L. (2014); *Pore structure of shale*. Fuel 143, pp. 467-475

Shabro V., Javadpour F., Torres-Verdin C. (2009); *A generalized finite-difference diffusive-advective (FDDA) model for gas flow in micro-and nano-porous media*. University of Texas, pp. 1-11

Sukop M.C., Thorne D.T. (2006); *Lattice Boltzmann modelling: An introduction for geoscientists and engineers*. Springer Verlag. 2006

Thorstenson D.C., Pollock D.W. (1989*); Gas transport in unsaturated zones: multicomponent systems and adequacy of Fick's laws*. Water Resour. Res., Vol 25, pp. 477-507

Webb S.W., Pruess K. (2003); *The use of Fick's law for modelling trace gas diffusion in porous media*. Transp. Porous Media, Vol 51, pp.327-341

Wei M., Duan Y., Fang W., Wang R., Yu Bo., Yu C. (2013); *Mechanism model for shale gas transport considering diffusion adsorption/desorption and Darcy flow*. J. Cent. South Univ. 20, pp. 1928-1937

Wu Q. (2014); *Investigation of fluids flow behaviour in nano-scale channels by using optic imaging system*. Doctoral Dissertations. Paper 2197

Zhang Y., Gu, X., Barber R.W., Emerson D.R. (2006); *Capturing Knudsen layer phenomena using a lattice Boltzmann model*. Physical Review E 74 (2006)

Zhang, X.L., Xiao, L.Z., Shan, X.W., Guo, L. (2014); *Lattice Boltzmann Simulation of Shale Gas Transport in Organic Nano-Pores*. Sci. Rep. 4, 4843

Zhang, X.L., Xiao, L.Z., Guo, L., Xie Q.M. (2015); Investigation of shale gas microflow with the Lattice Boltzmann method. Pet. Sci.

Nomenclature

A = cross-sectional area, m^2

D = Knudsen diffusion, m^2/s

F = theoretical dimensionless coefficient (adapted from Javadpour, 2009)

J = mass flux, $kg/s/m^2$

K = Permeability, m^2

L = pore throat length, m

M = molar mass, kg/kmol

p = pressure, Pa

q = flow rate, m^3/s

r = pore throat radius, m

R = gas constant, J/mol/K

T = temperature, K

Greek Letters

α = tangential momentum accommodation coefficient , fraction

μ = viscosity, Pa/s

ρ = density, kg/m3

Subscript

app = apparent

avg = average

D = diffusive

K = Knudsen